Darhad megaflood (southern Siberia): ause, age and consequence

Sergey Arzhannikov, Nastya Arzhannikova, Regis Braucher, Goro Komatsu

Darhad megaflood (southern Siberia): Cause, age and consequence

Sergey Arzhannikov[a,*], Anastasia Arzhannikova[a], Regis Braucher[b], Goro Komatsu[c]

[a]Institute of the Earth's Crust, Russian Academy of Sciences, Siberian Branch, 664033, Lermontova str., 128, Irkutsk, Russia

[b]CEREGE, Aix-Marseille Univ., CNRS-IRD UM34, Collège de France, INRAE, BP 80, 13545 Aix-en-Provence Cedex 4, France

[c]International Research School of Planetary Sciences, Dipartimento di Ingegneria e Geologia (INGEO), Università d'Annunzio, Viale Pindaro 42, 65127 Pescara, Italy

* Corresponding author.

E-mail address: sarzhan@crust.irk.ru (S. Arzhannikov).

Abstract

A combined geomorphological and geochronological investigation was carried out aiming at determining the cause of the Darhad paleolake formation and dating the Darhad megaflood. Based on the analysis of satellite image mapping, new data were obtained revealing conditions of glacial dams along the Shishkhid Gol valley. We hypothesize that large glaciers in Khara-Baryangiin Gol and Ikh-James Gol downstream of the Tengis Gol mouth were the main causes of the highest Shishkhid Gol backwater. The estimated height of this glacial dam there was about 300 m. The presence of paleolake shorelines at an altitude of 1713 m in the immediate vicinity of this glacial dam confirms its dominant role for the formation of the Darhad paleolake. Based on cosmogenic ^{10}Be exposure ages obtained on boulders from four fields of gravel dunes and of an erratic boulder exposed within a bar along the Yenisei River valley in the Tuva Basin, we infer that two among the three age peaks observed may correspond to megafloods at 36-38 ka and 18-23 ka.

Keywords

Southern Siberia; Late Pleistocene glaciation; Darhad paleolake; Darhad megaflood; Gravel dunes; ^{10}Be cosmic-ray exposure dating

1. Introduction

This study is aimed at identifying the cause-and-effect relationship regarding the Darhad megaflood, its age and role of shaping landforms in southeastern Siberia and northern Mongolia. The study of this phenomenon provides crucial information for understanding the development of topography and deposits in the area impacted by Quaternary glaciation and makes it possible to reconstruct paleolandscapes over a large area of northern Asia.

The global cooling in the late Pleistocene created conditions favorable for glaciation and advancement of glaciers over large areas both in polar regions and in mountain belts of the world. Within the ice sheets and in the territories adjacent to them, dammed proglacial lakes of various sizes with volumes up to several thousand cubic kilometers were formed. However, the subsequent climatic warming caused destruction of these glacial dams. The consequent glacial lake outbursts led to catastrophic discharge of water downstream. Discharges in some cases are estimated to be up to millions of m^3/s or more (O'Connor and Costa, 2004; Baker et al., 1993; Komatsu et al., 2009), and flood flows could have been up to 400-500 m deep (Rudoy, 2002).

In valleys and basins downstream of the proglacial lakes, specific relief forms of erosional and depositional origins were formed due to the floodwater passage (Baker, 1973; Baker et al., 1985, 1993; Carling et al., 2002; Komatsu et al., 2009; Margold et al., 2018; Benito and Thorndycraft, 2020). Erosive landforms include canyons, whirlpools, waterfalls, hanging valleys and spillways, and depositional landforms include gravel dunes and bars. Identification of these landforms have been used to indicate the past occurrence of megaflooding.

Three large paleolakes are known to be responsible for megaflood occurrence in the mountains of southern Siberia (fig. 1). These are Chuya-Kuray in Altay (Rudoy and Baker, 1993; Baker et al., 1993), Darhad in northern Mongolia (Grosswald, 1987; Komatsu et al., 2009), and Vitim in Transbaikalia (Margold et al., 2018). The collapsing of glacial dam is hypothesized to have led to the catastrophic discharge of water from the Darhad paleolake down the Yenisei valley, and this

is considered to be one of the largest megaflood events in the southern Siberian mountains (Grosswald, 1987; Komatsu et al., 2009, 2016; Batbaatar and Gillespie, 2016a). It is likely that the megaflood was multiple events and the estimated maximum peak discharge rate is ~3.5×10^6 m^3/s (Komatsu et al., 2009). The landscape formed by the Darhad megaflood is most fully represented along the Yenisei valley in northern Mongolia and the Tuva Republic (southern Siberia) (Komatsu et al., 2009, 2016; Arzhannikova et al., 2014). For instance, erosional and depositional landscapes formed by the megaflood are found extensively within the Kaa Khem Uplands and Tuva (Kyzyl) Basin. The study of megaflood landscape has made it possible to determine the conditions for flood hydraulics.

The chronology of the Darhad megaflood has been inferred mostly from the timing of the Darhad paleolake formation (Krivonogov et al., 2005; Gillespie et al., 2008; Komatsu et al., 2009; Batbaatar and Gillespie, 2016a, b). There have been limited attempts to determine the age of the Darhad megaflood from a set of geological data (Arzhannikova et al., 2014). However, detailed study has not been carried out yet to directly date the flood sediment.

There remain questions: in particular, 1) the precise timing of theDarhad megaflood, and 2) whether the Tengis Gol glacial dam was able to impound the deep Darhad paleolake. Our research is aimed at determining the timing of the Darhad megaflood and clarifying the conditions for the Darhad paleolake formation. We combine remote sensing mapping of geomorphology, geological studies, and in-situ ^{10}Be dating of exposed flood transported boulders. The work used topographic data from SRTM and TanDEM-X, geological survey maps of the USSR at a scale of 1:200,000, topographic maps at a scale of 1:100,000, and high-resolution satellite images available from Google Earth.

2. Study area

2.1 A brief history of paleolakes studies in Darhad Basin

The presence of ancient lacustrine sediments and coastlines in northern and northwestern Mongolia testifies for the widespread occurrence of paleolakes during the Quaternary (Selivanov, 1967; Spirkin, 1970; Grunert et al., 2000; Komatsu and Olsen, 2002; Arzhannikov and Arzhannikova, 2011; Stolz et al., 2012).

The largest was the proglacial Darhad paleolake in northern Mongolia (fig. 1). The lake was named after the depression in which it resided. This ice- or possibly sedimentary-dammed lake repeatedly formed in the Darhad Basin during the Pliocene and Pleistocene (Selivanov, 1967; Selivanov, 1968; Spirkin, 1970; Uflyand et al., 1971; Grosswald and Rudoy, 1996; Krivonogov et al., 2005; Gillespie et al., 2008; Komatsu et al., 2009). The morphology of the basin, surrounded by mountains peaking above 3000 m and the only runoff through the Shishkhid Gol, are the most favorable conditions for the formation of a lake basin.

According to Selivanov (1967), there were three stages in the formation of the paleolake. Two of them were associated with volcanic lavas and the last one with the Tengis glacier dam. The possible age of the existence of lakes is indicated only for the latter as the Lower-Middle Quaternary. Instead, Spirkin (1970) hypothesized that there had been three stages in the development of the paleolake: 1) Pliocene-Early Quaternary; 2) Late Quaternary - interglacial; 3) Late Quaternary - glacial (fig. 2).

According to some ideas (Spirkin, 1970; Uflyand et al., 1969), Darhad Basin was formed in the pre-Pliocene times (all dates are based on palynological analyses) or at the end of the Miocene and the beginning of the Pliocene, when the deformation front from the Indo-Asian collision reached this region (Jolivet et al., 2007). As a result of the mountain uplift to the west of the Darhad Basin, Shishkhid Gol was dammed, and a small lake was formed. Then, the river cut within the uplifted block, and the lake level lowered and the main elements of the valley were formed. Spirkin (1970) noted that during the interglacial period of the late Pleistocene (MIS3) the Shishkhid Gol valley had been dammed by volcanic lavas, leading to the formation of a small lake. However, $^{39}Ar/^{40}Ar$

dating of valley lavas showed an age of 6–4 Ma (Perepelov et al., 2017), which excludes the Quaternary age of the paleolake by the lava damming. It has been hypothesized that the lake reached its maximum level during the last phase of the Late Pleistocene glaciation (MIS2) due to damming of Shishkhid Gol by a Tengis glacier. The thickness of the terminal moraine reached 200 meters and the coastline of the paleolake was at 1700-1720 m asl (Spirkin, 1970). Further detailed studies of glaciation in the eastern Sayan and northern Mongolia significantly improved the chronology of glacier advances during the Late Pleistocene (Gillespie et al., 2008; Arzhannikov et al., 2012), and this led to a new discussion about the age of the glacial Darhad lake (Krivonogov et al., 2005; Gillespie et al., 2008; Komatsu et al., 2009; Batbaatar and Gillespie, 2016a, b).

2.2 Glacial-dammed Darhad paleolake

Researchers of Darhad Basin's Quaternary history have noted the widespread and well-preserved lake shorelines (Selivanov, 1967; Ufland et al., 1969; Ufland et al., 1971; Spirkin, 1970; Grosswald, 1987; Grosswald and Rudoy, 1996; Komatsu and Olsen, 2002; Krivonogov et al., 2005; Gillespie et al., 2008; Komatsu et al., 2009, 2016). On the slopes of the ridges in the basin, they are clearly traced up to a height of 1713 m asl (Krivonogov et al., 2005). Remote sensing data show that this level (1713 m asl) dominates throughout the Darhad Basin. The tops of the ridges and small extended ridges located within the basin have a system of encircling shorelines, which indicates the presence of islands during the existence of the Darhad paleolake (fig. 3).

Lake terraces are located on the slopes of the basin, river valleys, and on the escarpment of the Jarai terminal moraine. In total, there are 47 shorelines located on the right bank of the Shishkhid Gol (Tengis Gol mouth) (Krivonogov et al., 2005). According to observational data (Krivonogov et al., 2005; Gillespie et al., 2008; Komatsu et al., 2009), the lake shorelines are limited by the Tengis moraine (Tengis Gol mouth). Regarding the timing of the Darhad paleolake, there is no clear consensus on this matter. Gillespie et al. (2008) believe that the glacier advances from the

mountains around the Darhad Basin occurred at 17-19 ka, 35-53 ka, and at least one more time earlier. Krivonogov et al. (2005) consider that a large lake was formed 110-116 ka and probably existed until 15 ka, changing in size with time.

Geological and geomorphological analyses, mapping and dating of Quaternary deposits showed that the possible reason for the formation of the Late Pleistocene Darhad lake could have been glaciers emerging from lateral tributaries of Shishkhid Gol (fig. 4), blocking the river flow down the valley (Grosswald and Rudoy, 1996; Krivonogov et al., 2005; Gillespie et al., 2008; Komatsu et al., 2009, 2016). Krivonogov et al. (2005) considered one glacial dam in the area of the Tengis Gol mouth. According to Gillespie et al. (2008), there were probably two glacial dams at the outlets of Tengis Gol and Gadar-Usiyin Gol. Komatsu et al. (2009) and Batbaatar and Gillespie (2016a) hypothesized three glacial dams. The most downstream of them was located at the mouth of the Barangiin Gol. Highlighting different numbers of glacial dams, the researchers nevertheless agreed that the main reason has been the glacier advancing from the Tengis Gol valley. The glaciers downstream of Shishkhid Gol were thinner and could not account for the deep Darhad paleolake (fig. 4) (Grosswald and Rudoy, 1996; Krivonogov et al., 2005; Gillespie et al., 2008; Komatsu et al., 2016).

2.3 The Darhad megaflood

While studying the glacial landscape of the Sayan-Tuva uplands (southern Siberia), scientists discovered landforms resembling gravel dunes. Borisov and Minina (1982) characterized them as ribbed and cellular ground moraines, an element of the Middle Pleistocene glaciation. However, the advent of publications about gravel dunes found in Altai (Baryshnikov, 1979; Butvilovsky, 1982; 1985; Rudoy, 1984) and claiming them as the important elements of major hydrological catastrophes (megafloods) initiated a search for similar landforms in other regions of mountains in southern Siberia. The first geologist who recognized the complex of erosional-depositional

forms in the Yenisei valley as the result of high water discharge from the Darhad paleolake was M.G. Grosswald. By comparing the data on the Darhad paleolake with a giant canyon (coulee) carved in volcanic lavas and a system of gravel dune fields in the Tuva Basin formed in the glacial time, Grosswald (1987) concluded that megaflooding had occurred in the past. Since then, the Darhad phenomenon has attracted attention of the world scientific community. Various studies were conducted, and field conferences were held. Some articles have been published on the morphology, water flow dynamics and velocity, flow modeling, paleogeographic reconstruction, etc. (Grosswald, 1987; Grosswald, 1996; Krivonogov et al., 2005; Gillespie et al., 2008; Komatsu et al., 2009, 2016; Arzhannikova et al., 2014; Batbaatar and Gillespie, 2016a, b).

3. Methods

3.1 Mapping

The production of geomorphological maps and schemes for the study area was based on relief hillshading and visual interpretation of remote sensing data (SRTM V4 (spatial resolution 90 m), ALOS (spatial resolution 30 m), TanDEM-X DEM (spatial resolution 12 m); topographic maps, geological maps, satellite and aerial photographs of various scales) and published data (Krivonogov et al., 2005; Gillespie et al., 2008; Komatsu et al., 2009, 2016; Batbaatar and Gillespie, 2016a, b). Satellite image analysis, identification of landforms and mapping were carried out in programs Google Earth and QGIS. The analysis was carried out on the territory of the Yenisei valley and the adjacent areas spanning over the Darhad Basin to the Sayano-Shushenskoye reservoir. Attention was paid to the study of the lake terrace complex and glacial landforms located in the Darhad Basin and in the Shishkhid Gol valley. In order to obtain information about the Darhad megaflood, Yenisei terrace complexes and gravel dune fields in the Tuva Basin were analyzed in detail.

192 The process of mapping proceeded as follows. The primary analysis was conducted based on
193 SRTM (spatial resolution 90 m) data. Then, ALOS data (spatial resolution 30 m) and TanDEM-X
194 DEM data (spatial resolution 12 m) were also used. Using Google Earth and QGIS we
195 superimposed satellite images of various scales (Google Earth and QGIS) on topographic data to
196 obtain high-quality three-dimensional imagery. This way, we were able to perform a detailed
197 analysis of erosional and depositional features caused by the megaflood. Landforms associated
198 with other lithological factors (i.e., not by the megaflood) were excluded using geological maps.
199 Geological data also provided information on the extent of Quaternary deposits, which was
200 important in interpreting the distribution of Darhad megaflood sediments. Topographic maps were
201 the source of information regarding names of main topography in the study area, as well as the
202 basis for the correcting absolute heights (m asl) for radar-derived topographic survey data (SRTM,
203 ALOS, TanDEM-X DEM). Due to the fact that all radar data have errors in altitude, we checked
204 the control points (trigopoints) on topographic maps, and if there were errors, we made a
205 correction.
206
207 **3.2 ^{10}Be exposure dating**
208
209 We used beryllium (^{10}Be) in-situ dating (Wagner, 1998; Gosse and Phillips, 2001) to determine
210 the age of exposed gravel dune boulder surfaces. The accumulation of ^{10}Be atoms occurs under
211 the action of cosmic rays on the surface of rocks. It accumulates in silicate minerals, especially
212 quartz, and is therefore suitable for dating exposed surfaces. Since the in-situ production in quartz
213 (bedrock: granite, quartzite, quartz vein) is low (~4 at/gSiO_2/y) (Borchers et al. 2016), 10–30 g of
214 quartz is required for analysis (Wagner, 1998). The half-life of (^{10}Be) is 1.387 Ma (Chmeleff et
215 al., 2010; Korchinek et al., 2010), which makes it possible to date surface rocks over a wide time
216 range.

One of the main conditions for obtaining high-quality data is the immobility of the dated boulder from the moment of its exposure. The boulder exposure should coincide with the end time of the megaflood, and its location (orientation in space) should be maintained until the moment of sampling. However, from the moment of exposure, exogenous processes begin to work, affecting its safety and stability on the surface of gravel dunes. These include river erosion (bottom and side), thermokarst, solifluction, denudation, wind action and desquamation. Bottom and side erosion of streams significantly deforms the surface of gravel dunes. However, water erosion is localized in a narrow area, forming a valley that is excluded from the sampling sites. The development of thermokarst leads to surface deformation and the appearance of small depressions. Near-horizontal surfaces of a large area indicate the absence of any active thermokarst processes within them for a long time and the boulders in the area can be used for sampling.

Another factor that can affect the accuracy of determining the exposure of a sample is its shielding of the surrounding topography. The degree of topographic shading can be determined by simple circular measurement of the angles and strike of shadow sectors from mountain peaks or extended ridges, which is taken into account later in dating (Gosse and Phillips, 2001).

3.2.1 Sampling

Four fields of gravel dunes were chosen for sampling, located over a distance of 150 kilometers along the Yenisei valley (fig. 13 c, d). A peculiar attention was paid to the sample position at a maximum distance from nearby slope to exclude solifluction flow and at where no thermokarst is observed. The geographic position and altitude of each sample were obtained using a portable GPS (horizontal uncertainty ±5m). The topographic shielding was also measured for each sample.

Gravel dune field I (51°33.883N; 93°59.016E) (fig. 5 a) is located on the right bank of the Yenisei River and its dimension is 8 x 2 km. Gravel dunes occur at several terrace levels with a total area of 11.5 km^2. The maximum level above the Yenisei River is 30-40 m, the minimum level

is 14-16 m. The continuous transition of gravel dunes from higher to lower levels indicates their simultaneous formation. The presence of a depression in the rear part of the dunes in the area of contact with the slope and its absence at the head of the dunes indicates possible existence in the past of a terrace level 10–12 m high, buried during the Darhad megaflood. This fact implies a thick deposit (~20 m) formed by the Darhad megaflood in this part of the Yenisei valley. The swell-like structure of the dunes is distinguished in the longitudinal and transverse profiles. Ridges 1-2 m high prevail on the surface of the gravel dunes and their heights increase towards the central part up to 6-8 m. 5 samples (Tuva-16-1, 2, 3, 4, 5) were taken from the surface of boulders located in the dunes.

Gravel dune field II (51°43.101N; 94°33.670E) (fig. 5 b) is located on the right bank of the Yenisei River. There are two levels of gravel dunes at 35 and 70 m. The total area is 12 km^2. The height of the gravel dune ridges is on average 2-4 m, or rarely reaching 4-6 m. On the surface, many boulders up to 1 m in size, and in some places 2-4 m, are found everywhere. In the eastern part of Gravel dune field II, 5 samples were taken from the surface of boulders (Tuva-16-6, 7, 8, 9, 10).

Gravel dune field III (51°40.020N; 94°53.032E) (fig. 5 c). This is one of the largest gravel dune fields in the Yenisei valley. It is located on the right bank of the river. Its area is more than 20 km^2. The gravel dunes are positioned at three levels at 14, 30-40 and 70 m relative to the Yenisei River. 5 samples (Tuva-16-12, 13, 14, 15, 16) were taken from the surface of boulders on a gravel dune located on the 30 m terrace.

Gravel dune field IV (51°40.020N; 94°53.032E) (fig. 5 c). The sampling field is the surface of a gravel dune located 14 m above the current water level in the Yenisei River. The height of the ridges is 0.5-0.7 m. 5 samples were taken from this level (Tuva-16-17, 18, 19, 20, 21).

An additional sample was obtained from, the bar area (51°18.397N; 95°44.375E) (fig. 5 d), on the right bank of the Yenisei River, in the western part of the Kaa Khem Uplands. This sample (Tuva-16-11) was taken from a boulder measuring 8 x 4 m and 2-2.5 m high. The mass of the boulder is

estimated to be about 172 tons. The sampling point is located on the 25 m terrace. The dimensions of the granite boulder testify for the significant power of the water flow, as the nearest bedrock of granites is located 15 km upstream.

Overall, we collected 21 samples from the surface of gravel dunes with heights of 12-14 m, 30 m, 40-50 m and from the surface of a 25 m terrace within the bar.

3.2.2 Samples preparation and measurements; Exposure ages calculation

Samples preparation was done at LN2C, the French National Laboratory for Cosmogenic Nuclides located at CEREGE (Aix en Provence).

Samples were crushed and sieved (0.25 to 1 mm fraction) then purified with a mixture of hydrochloric and fluorosilisic acids (2/3 – 1/3 ratio) until pure quartz was obtained. Three leaching steps in diluted HF were then performed to eliminate the adsorbed atmospheric ^{10}Be, resulting in the loss of ~30% of the initial material.

A weighed amount (~0.1 g) of ^{9}Be solution (3025±9 ppm) was added to the decontaminated quartz. Beryllium was subsequently separated from the solution by successive anionic and cationic resin extractions and precipitations. The final precipitates were dried and heated to 800°C to obtain BeO which was finally mixed with niobium powder prior to analysis by Accelerator Mass Spectrometry at ASTER (Cerege, Aix en Provence). The beryllium data were calibrated directly against STD11 standard (Braucher et al., 2015) with a ^{10}Be/^{9}Be ratio of 1.191×10^{-11} (±1.09%). Uncertainties on measurements include the counting statistics, the standard variability during the run, the uncertainty on STD11 standard (1.09%) and an external machine uncertainty of 0.5% (Arnold et al., 2010). ^{10}Be/^{9}Be samples ratios are 8 to 82 times higher than the chemical blank ratio (5.8×10^{-15}).

To calculate the exposure ages, a sea level high latitude production rate of 4.02 at/g/a was used and scaled to the latitude and altitude of the studied area using the Stone (2000) polynomial law. The muons scheme follows Braucher et al. (2011).

The general equation used to model ^{10}Be concentrations considering the three types of particles involved is given by eq. (1):

$$N(x,\varepsilon,t)= \frac{P_n.e^{-\frac{\rho x}{\Lambda_n}}.\left(1-e^{\left(-t\left(\frac{\rho\varepsilon}{\Lambda_n}+\lambda\right)\right)}\right)}{\frac{\rho\varepsilon}{\Lambda_n}+\lambda}+\frac{P_{slow}.e^{-\frac{\rho x}{\Lambda_{slow}}}.\left(1-e^{-t\left(\frac{\rho\varepsilon}{\Lambda_{slow}}+\lambda\right)}\right)}{\frac{\rho\varepsilon}{\Lambda_{slow}}+\lambda}+\frac{P_{fast}.e^{-\frac{\rho x}{\Lambda_{fast}}}.\left(1-e^{-t\left(\frac{\rho\varepsilon}{\Lambda_{fast}}+\lambda\right)}\right)}{\frac{\rho\varepsilon}{\Lambda_{fast}}+\lambda} + N(0,\varepsilon_2).e^{-\lambda t} \quad \text{(eq.1)}$$

where $P_{n.}$, $P_{stop.}$ and P_{fast} are the production of neutrons, stopping and fast muons respectively, ρ is the material density, □□is the denudation rate (set to zero in this study), t is time, Λ_{neut}, $\Lambda_{stop.}$ and Λ_{fast} are the attenuation lengths of neutrons (150g/cm^2), stopping (1500 g/cm^2) and fast muons (4320 g/cm^2), respectively. The term $N(0,\varepsilon_2)$ is a potential inheritance coming from a previous exposure. λ is the radioactive decay constant (λ = ln2/half-life).

4. Results

4.1 The water level of the Darhad paleolake according to the interpretation of satellite images and radar-derived topographic data

The analysis of shorelines of the Darhad paleolake based on satellite images and SRTM data shows that the highest coastline of the paleolake corresponds to an altitude of 1713 m asl. The most interesting result of remote sensing in the area of the Shishkhid Gol valley is the presence of shorelines of a paleolake observed downstream of the Tengis Gol mouth. These shorelines are well identifiable on the slopes of the valley up to a height of 1713 m asl. For example, on the right bank

side of the Shishkhid Gol valley, 12 km downstream the Tengis Gol mouth, lake terraces are clearly visible, tracing slopes of the main valley and partially visible on slopes of lateral tributaries (figs. 5, 6). Several shoreline features are clearly visible starting from the Tengis mouth down the Shishkhid Gol valley (figs. 6 a, b, c, d, 7). Each extended shoreline visible on the satellite image corresponds to an isoline, with its characteristic height, determined from the SRTM and ALOS data and refined from the topographic maps of the USSR.

Shoreline group I (fig. 6 a) is located 2.2 km downstream of the Tengis mouth. The slope of the valley is terraced along a distance of 1.2 km between 1680 and 1713 m asl. Shoreline group II (fig. 6 b) is located in the valley of the right lateral tributary of Shishkhid Gol. On one of the capes formed by the main valley and tributary, a series of shorelines 1.4 km long is visible, and they are positioned from 1640 to 1713 m asl. Shoreline group III (fig. 6 c) is located 7 km downstream from the Tengis Gol mouth. On the slope of the western exposure, the terrace levels of the paleolake, 0.7 km long, are clearly visible at two levels. They are concentrated between 1550 and 1713 m asl. Shoreline group IV (fig. 6 d) is located 12 km downstream from the Tengis Gol mouth. On the slope of the right tributary in its mouth part, a series of parallel coastlines 1 km long is clearly visible. They are positioned between 1520 and 1713 m asl. An abraded slope 1.2 km long downstream from the mouth of this tributary is also clearly visible (fig. 6 d).

The shorelines were formed also on a slope in the Sarig Gol valley (the left tributary of Shishkhid Gol). Furthermore, there is a fragment of the Tengis terminal moraine (fig. 8 f). This indicates that the height of the Tengis glacier, which dammed the Shishkhid Gol valley, did not block it up to the height of 1713 m asl. This should have allowed the formation of a paleolake bay in this valley, which is marked by Krivonogov et al., 2005. In Darhad Basin, in the border parts and in the inner area, there are small ridges and hills. During the existence of the paleolake, they were peninsulas and islands. Coastal ridges and terraces formed on their slopes when the water level changed.

343 Analysis of satellite images and DEM data showed that the highest paleoshoreline was not
344 constant in elevation and varied from 1713 m asl down to 1686 m asl (figs. 7, 8). For example, the
345 upper lake line is traced at an altitude of about 1705-1703 m asl on the southern slopes of a small
346 ridge located north of Dood-Nur and Targan-Nur lakes (fig. 8 g, h, j, k). If we move to the
347 southwest, we see that the height of the upper coastline changes to 1696 m asl, and further south
348 it changes to 1686 m asl (fig. 8 l, m). Thus, the change of the upper paleolake shoreline elevation
349 possibly indicates significant tectonic deformations within the Darhad Basin that have occurred
350 since its drainage.
351
352 **4.2 Tectonic and gravitational deformations**
353
354 The Darhad Basin is part of the southwestern segment of the Baikal rift zone and is
355 characterized by its latitudinal extension. The Darhad Basin is controlled by normal faults
356 extending from the east and west. The thickness of the sedimentary cover is 300-400 m (Logachev,
357 1993). The analysis of satellite images and DEM data made it possible to detect seismogenic
358 ruptures and gravitational displacements within the Darhad lake basin (fig. 9). The activation of
359 faults apparently occurred both during the existence of the lake and after its drainage. In the
360 northern part of Darhad Basin, a fault of meridional strike was found with a displacement
361 amplitude from 25 m in the south to 60 m in the north. The displacement along the fault led to
362 partial subsidence and burial of the Khogorgyn Gol valley (fig. 9 a). A latitudinal normal fault
363 with a displacement amplitude of about 50 m is located to the north of Lake Dood Tsagan Nur. It
364 extends from the Khogorgyn Gol valley, crossing the southern part of the meridional fault and
365 ends in the region of Lake Targan-Nur (fig. 9). Another complex of deformations is located to the
366 east and is represented by a NE-trending scarp on the southern slope of a small ridge (fig. 9 b).
367 The revealed seismogenic faults in the eastern part of the Darhad Basin (fig. 7), in the area of
368 the Jarai terminal moraine (Logachev, 1993), indicate ongoing active tectonic movements in this

area. Seismogenic ruptures with a maximum amplitude of 8 m displaced proluvial, colluvial, and glacial deposits. The length of the fault visible on the surface is 13 km. Along with the faults displacing bedrock and sedimentary deposits, landslides are widespread, which are located at the foot of small ridges within the Darhad Basin.

4.3 Reconstruction of glacial dam No. 1 at the Tengis Gol outlet

The main landforms that help in reconstructing dimensions of a glacier are terminal and lateral moraines, spillways and meltwater channels. The absolute height of the left (1715-1737 m asl) and right (1720-1745 m asl) lateral moraines located at the Tengis Gol mouth and the height of the spillway thalweg (1700-1740 m asl) suggest the possibility of dam formation in the Shishkhid Gol valley by the Tengis glacier (Krivonogov et al., 2005; Gillespie et al., 2008; Komatsu et al., 2009, 2016; Batbaatar and Gillespie, 2016 a, b;). This is confirmed by the fact that some part of the terminal moraine is located on the opposite side of Shishkhid Gol at the mouths of its left tributaries. Here, the absolute height of the terminal moraine is 1640 m asl. We can assume that there were two levels of standing of the Tengis glacier in MIS2, based on the presence of spillways with different absolute heights in the mouth part of Tengis Gol and also ^{10}Be ages (Gillespie et al., 2008; Batbaatar and Gillespie, 2016b).

The Level I standing of the Tengis glacier is determined by upper spillways (1700-1740 m asl), fragments of the terminal moraine (1640 m asl), abraded slopes and meltwater channels on the right and left banks of Shishkhid Gol (fig. 10 a, b, c, d). The Level II standing can be reconstructed from a lower spillway (1657 m asl) and lake terraces located on the slopes at the Tengis Gol mouth (fig. 11). Level I in front of the Tengis Gol mouth had a height of 1750 m asl. However, as the Tengis glacier entered the Shishkhid-Gol valley, its level dropped to 1650 m asl. This is the height of the terminal moraine and the height of the upper part of the abraded slope on the left bank of Shishkhid Gol (fig. 10, profiles AB, CD). The exposure age of the terminal moraine in the Sarig

Gol valley (Batbaatar and Gillespie, 2016b) characterizes the glacier advance in the LGM (MIS2). The reconstruction of the Tengis glacier on profile CD (fig. 10) shows that Level I on the left bank of Shishkhid Gol was significantly lower than the maximum (1713 m asl) transgression of Darhad paleolake.

Paleolake terraces are widespread on the right slope of the Shishkhid Gol valley at the mouth of the Tengis Gol. They abrade the surface of glacial deposits of Level I. The terraces are not covered by moraine deposits (fig. 11). Their location and height suggest a significant decline in the glacial level (meltwater channel 1657 m asl, fig. 11). The exposure age (^{10}Be, 20.7±1.1, 18.2±1.0 ka) of the melt water channel (Gillespie et al., 2008) agrees with MIS2 after LGM (fig. 11). The AB and CD profiles (fig. 11) show a significant reduction in the Level II ice within the Tengis dam.

4.4 Glacial features and parameters of glacial dam No. 4 at the Khara-Baryangiin Gol and Ikh-Jams Gol mouths (right and left tributaries of Shishkhid Gol)

Khara-Baryangiin Gol is the right tributary of Shishkhid Gol (fig. 4). The valley is located within a mountain range with elevations over 3000 m asl. Glacial cirques and troughs are widespread in the upper reaches of this river basin. There are different levels of lateral moraines on the slopes of the valleys. In the mouth part of the river there is a large terminal moraine, and there are lateral moraines in the valley. They are clearly visible both on satellite images and on the ALOS DEM. The absolute height of the left lateral moraine in the Khara-Baryangiin Gol valley (at the mouth) is 1890 m asl (figs. 4, 12 a).

Ikh-James Gol is the left tributary of Shishkhid Gol. The ice-catchment is located within a mountain range with elevations of 2700-3000 m asl. On the slopes of the river valley, fragments of lateral moraines have been preserved, giving information about the thickness (300-500 m) of

420 the glacier. The elevations of the glacier at the mouth on the left and right slopes are 1770 m asl
421 and 1745 m asl, respectively (fig. 12 b).
422 The mouths of these tributaries (Khara-Baryangiin Gol and Ikh-James Gol) are located opposite
423 to each other. The glaciers joined in the Shishkhid Gol valley and formed a large glacial dam with
424 the level corresponding to 1715-1720 m asl (fig. 12 c). The altitude of the glacial dam is determined
425 from the elevation of the melt water channel (fig. 12 d) on the left side of Shishkhid Gol. Additional
426 evidence for the presence of a glacial dam is a series of erosional grooves on the slope, which
427 record a decrease in the elevation of the glacier in this part of the Shishkhid Gol valley.
428
429 **4.5 The main erosional and depositional landforms of the Yenisei valley**
430
431 The Yenisei valley in the Tuva Basin (fig. 1 b) presents the existence of two main erosional-
432 depositional landforms formed during and after the Darhad megaflood (fig. 13). The main
433 landscape elements formed after the Darhad megaflood include low and high floodplains (fig. 13
434 c, d), which have special features distinguishing them from other erosion-depositional forms. The
435 combination of bottom and lateral erosion led to the formation of clearly defined escarps of
436 terraces, meanders and oxbow lakes. The seasonal rise of water in the river resulting from rains
437 and melting of snow lead to changes in channel configuration, death of old and birth of new
438 meandering channels and islands.
439 The second complex of erosional-depositional landforms is positioned 12 m above the low
440 relief (fig. 13 c, d). The distinguishing characteristics are the absence of meanders and the presence
441 of linear structures on the surfaces of high terraces, which indicates the formation of this relief
442 with certain dynamic conditions. These linear structures are a system of gravel dunes (or giant
443 current ripples, terminology in old literature) (fig. 13) as described in Komatsu et al. (2009), who
444 also documented their morphology, topographic setting and correlations with megaflood
445 hydraulics.

446 The nature of the Yenisei valley within the Tuva Basin predetermined the wide distribution and
447 preservation of terraces of various levels. Some of them were formed by the Yenisei cutting into
448 deposits of the Darhad megaflood; in other cases, megaflood deposits cover or lie on the surface
449 of ancient terraces. The width and length scales of the terrace surfaces are kilometers and even a
450 few tens of kilometers. In the Yenisei valley, there are a low floodplain (2–4 m), a high floodplain
451 (6–8 m) and terrace levels of 12–14, 18–20, 30, 40–50, and 100 meters (fig. 13). On all levels of
452 the terraces, except for the low and high floodplains and the 100 m level, gravel dune fields are
453 observed. There is even a level of gravel dunes located at an altitude of 70 m above the level of
454 the Yenisei River.
455
456 **4.6 Water level and depth of the Darhad megaflood in Tuva Basin**
457
458 Based on the analysis of satellite images and DEM data, we discovered and subsequently
459 examined in the field a series of terraces formed in the process of lateral erosion during a decrease
460 in the water level of the paleoflow along the Yenisei valley (fig. 14 c). These terraces are horizontal
461 levels, more than 5 km long, and formed into colluvial-diluvial deposits overlying Jurassic
462 sedimentary rocks and Paleozoic granodiorites (fig. 14 a, b). It should be noted that we are talking
463 about high-level terraces (about 100 m, relative to the current water level in the Yenisei River).
464 In total there are 7 levels of different preservation. The highest of them were recorded at a
465 height of 725 m asl. In (fig. 14 a, b), and elements of terraces with well-defined horizontal surfaces
466 and escarps are clearly visible both from the Yenisei side and in temporary streams. Such relief
467 elements can often be seen on the slopes of artificial reservoirs with seasonal fluctuations in water
468 levels. The terraced surface contains poorly rounded fragments of various metamorphosed and
469 igneous rocks. Outcrops of Jurassic rocks are located in the lower part of the ledge of a 50-meter
470 terrace. Analysis of geomorphological profiles (fig. 14 c, d) drawn along lines AB and CD
471 covering the complex of terraces and different levels of gravel dunes showed that the depth of the

Darhad megaflood stream above the present level of the Yenisei River was 90-100 m and above the lowest level of gravel dunes at 60-65 m.

4.7 Morphological analysis of gravel dunes

A large volume of water and various topographic conditions of the Yenisei valley (from wide depressions to narrow canyons) along the path of the glacial superflood created a complex of erosion-depositional landforms. First of all, it is necessary to note that fields of gravel dunes are widespread in the Tuva Basin. Gravel dunes are a system of extended ridges and depressions oriented perpendicularly or at an angle to the general direction of the water flow (fig. 15 a, c). Gravel dunes are composed of sand, gravel, pebbles and boulders (fig. 15 b). And the composition varies within a single gravel dune field, which is influenced under conditions of different water flow rates.

On the surface of the gravel dunes many boulders up to a few meters in diameter can be encountered. Sometimes there are stone "monsters" up to 8-10 m in size. The basalt fragments found in gravel dune surfaces showed that the movement of boulders 0.5-1 m in size (fig. 16 f) could have occurred over a distance of over 100 km. The height of the gravel dunes varies from 1-2 m to 6-7 m. Their length can reach several hundred meters. These gravel dunes are essentially bedforms of diluvial flows. The main area of gravel dune formation is concentrated in Tuva Basin along the Yenisei valley from the Kaa Khem Uplands to the river's entrance to the canyon of the Western Sayan Ridge (fig. 13 c, d). The total length of the river stretch with observed gravel dune fields reaches for more than 200 km, and their number approaches two dozen.

The periodicity of the Darhad paleolake formation (Gillespie et al., 2008; Komatsu et al., 2009) suggests that there could have been several catastrophic discharges of water from this lake. The surviving gravel dune fields are in many cases located in the stream shadow zone created by the bend of the river and the protruding cape of bedrock as observed by Komatsu et al. (2009). In some

cases, in the zone where gravel dune deposits adjoin bedrock slopes, there are depressions in the relief, representing a through or blind valley, on the surface of which gravel dunes are also located. The granulometric composition of the gravel dunes ranges from pebbles mixed with boulders to gravel and well washed horizontally-lying sand. Coarser sediment is often found in areas of shade along river bends. Downstream of the river, the dimension of alluvium decreases to gravel and sand fractions.

The deposits formed by the Darhad megaflood are concentrated within the Tuva and Minusa Basins, and partly in the river valleys located in the Western Sayan Ridge and Kaa Khem Uplands (Komatsu et al., 2009, 2016; Arzhannikova et al., 2014). The deposits are represented by clastic material of various sizes: sand, gravel, pebble, boulder and hummock (fig. 16 a-g). Sandy sediment occurs as large in-situ units (fig. 16 a, b) and as heavily wind-blown (fig. 16 c) (aeolian sand units). In-situ sand units are usually located in the narrowing zones of the valley, in the peripheral mouth parts of lateral tributaries, and at the exits from narrow valleys into its wide parts or into depressions (Arzhannikova et al., 2014). A typical in-situ sand unit (6–8 m) located on the right bank of the Yenisei valley is represented by horizontally stratified deposits of various thicknesses from 2–3 mm to 15–20 cm with inclusions of rare pebbles (fig. 16 a), which occur on pebbles and covered with loess-like light sandy loams.

In sandy deposits, there are blocks that are also composed of sand, however, having a different texture from their surrounding sediments. The intactness of the blocks suggests their frozen state during transport by water, as evidenced by subsidence of overlying sediments after the blocks have melted and compacted (fig. 16 b). In some cases, unconformities of sands with underlying sediments are recorded (fig. 16 b). Perhaps they indicate multiple episodes of discharge from the Darhad paleolake.

Aeolian sand unit are located both in the Yenisei valley and beyond. They were formed by intense eolian processes. In present day, some units of sand sea (fig. 16 c) are located 100 km from their original formation site.

524 Gravel and pebble units are widespread within gravel dunes (fig. 16 d, e). In some sections,
525 deformed gravel deposits with rare large pebbles overlain by sandy loams are recorded. Such
526 deformations are recorded in deposits about 1 m thick. They may be associated with strong paleo-
527 earthquakes and represent seismic convolutions. A high degree of seismic activity is indicated by
528 numerous falls in mountainous areas in the immediate vicinity of the deformed deposits.
529 Boulder units are located in terrace outcrops and on the gravel dune surfaces. Their sizes vary
530 from 0.5 m to 1 m (fig. 16 f, g). Some of them are well rounded and have a spherical or ellipsoidal
531 shape. Other boulders have a low degree of roundness and are represented by angular large
532 fragments.
533 Hummock units occur within gravel-pebble deposits and on the surface of gravel dunes (fig. 16
534 h, g). The size of such fragments reaches 8 m.
535
536 **4.8 ^{10}Be surface exposure dating**
537
538 For the gravel dunes in the Yenisei River valley, the exposure age was obtained for 19 samples
539 out of 21 selected. Two samples did not have enough quartz for dating. The exposure age was
540 distributed over a large time range from 137.5 to 18.6 ka (table 1). We interpret these ages to
541 reflect the formation timing of the gravel dunes and thus approximate the formation chronology
542 of the Darhad megaflood.
543 The samples were collected from terrace surfaces with height levels of 40, 30, 25 and 15
544 m (fig. 13 c, d) with the intention to determine exposure ages of boulders composing gravel dunes
545 at various topographic positions.
546 The Gravel dune field I samples (T1, T3, T4, T5) obtained in the western part of the Yenisei
547 River valley (fig. 13 c) has a significant scatter of exposure ages (Table 1). The oldest of them at
548 ~79.5 ka (T1) and ~137.5 ka (T5) were sampled from bedrock granitic rocks located within the

549 gravel dunes. There are two samples (T3, T4) taken from boulders that have similar exposure ages
550 of ~31 ka and ~30 ka and the ages belong to the final MIS3.

551 The Gravel dune field II samples (T6, T7, T8, T9, T10) were located on the surface of a
552 30-m terrace 45 km east of the I group (fig. 13 d). The ages of these samples refer to the periods
553 of MIS 3 and MIS 2. The closest ages are for samples T7 (~26.9 ka) and T10 (~27.8 ka). It is
554 possible to distinguish samples T6 (~31.1 ka) and T8 (~37.6 ka), which are also close in time. The
555 T9 sample has a younger age of ~18.6 ka. The sample T11 was taken from a large boulder at the
556 eastern edge of the gravel dune fields (fig. 13 d). The exposure age of this sample is ~20.3 ka and
557 it can be considered valid and reliable (even though it is a single sample) since its position and
558 dimension (fig. 16 j) exclude movement of the boulder during the entire history of its exposure.

559 The Gravel dune field III samples (T12, T13, T14, T15, T16) were located on a 30-m high
560 terrace (fig. 13 d). The exposure ages of the boulders have a significant scatter ranging from ~94.7
561 ka to ~20.2 ka, which indicates a complex exposure history.

562 The Gravel dune field IV samples (T17, T18, T19, T20) were located on a 15-m high
563 terrace (fig. 13 d) and they are characterized by a significant scatter of exposed ages ranging from
564 ~72.6 ka to ~23.7 ka. The samples T18 (~23.7 ka) and T20 (~29.3 ka) have the closest ages.

565 Our exposure age analysis of the gravel dune surfaces shows a significant time spread. In some
566 cases, older age is likely because the sample was taken from a remnant of bedrock embedded
567 within the gravel dunes. The wide time range might also be indicative of a complex exposure
568 history associated with significant movements in space of the dated boulders. On the time scale,
569 older samples are represented by dates ranging from 137 ka to 51 ka (fig. 17 b). These samples
570 were ignored in further analysis because they should have significant inherited numbers of atoms.
571 The rest of the samples make up three age groups (three peaks): series of the samples I is 36-38 ka
572 (3 samples) corresponding to MIS3; series of the samples II is 27-31 ka (7 samples) corresponding
573 to MIS3-MIS2; series of the samples III is 18-23 (4 samples) corresponding to MIS2.

574

5. Discussion

5.1 Conditions of the Darhad paleolake formation

The existence of paleolakes in the Darhad depression during the Late Pleistocene is recorded from ancient lacustrine terraces and a sedimentary complex. The main backwater site for the Darhad paleolake has been considered to be the Tengis Gol mouth, where traces of a glacial dam are preserved (Krivonogov et al., 2005; Gillespie et al., 2008; Komatsu et al., 2009; Batbaatar and Gillespie, 2016a).

However, our newly discovered evidence for the existence of a paleolake extension downstream of the Tengis Gol mouth (fig. 6) indicates a more complex system of dams in the Shishkhid Gol valley than it was previously accepted. The lake shorelines discovered below the Tengis dam are identical in elevation (1710-1713 m asl) to the maximum level of the Darhad paleolake (fig. 7). In this case, a question arises whether the Tengis glacier was the main dam for the Darhad paleolake? Determining the parameters of the glacier based on the elements of the glacial features at the Tengis Gol mouth is important for checking the possibility of forming a glacial dam for the formation of the Darhad paleolake.

At the Tengis Gol mouth there are glacial and lacustrine features. Glacial features include lateral moraines, terminal moraines and meltwater channels. All of them provide information about the parameters of the glacier. The lacustrine features include ancient shorelines preserved on the slopes of Shishkhid Gol testifying for the level and water contact with bedrock (figs. 10, 11).

The elevation of the lateral moraines at the Tengis Gol mouth, exposure age of the terminal moraine at the left tributary, melt water channels, and lake shorelines on the slope of the Shishkhid-Gol valley provide evidence for two elevational levels of the glacial dam at MIS 2 (figs. 10, 11). This has been pointed out (Gillespie et al., 2008) by giving the upper glacial level an older indeterminate age. The exposure age of boulders (20.8±1.1 ka and 18.2±1.0 ka) within the melt

601 water channel (Gillespie et al., 2008) characterizes the late stage of development of the Tengis
602 glacier (fig. 11). The exposure age of boulders (23.8±1.5 ka and 20.7±1.4) from the terminal
603 moraine (fig. 10 d) of the left tributary of Sarig Gol (Batbaatar and Gillespie, 2016b) belongs to
604 the early stage and correlates with LGM. However, based on the reconstruction results, doubts
605 arise whether the Tengis glacier could really have been a dam for the Darhad paleolake, since the
606 observed shorelines of the paleolake there are positioned at higher elevations than the surface of
607 the glacier (figs. 10, 11).

608 The analysis of satellite images and topographic data provided new information on the
609 conditions of formation and size of the Late Pleistocene Darhad lake. The existence of abrasion
610 lake levels upstream and downstream of the Tengis dam, as well as their coincidence in elevation
611 (1713 m asl), suggests the presence of a large backwater below the confluence of Tengis Gol and
612 Shishkhid Gol. We identified the confluence area of the Khara-Baryangiin and Ikh-Djams glaciers
613 as a likely backwater site (fig. 12). Here a large 300-m high dam was formed in the Shishkhid Gol
614 valley. Prior to this work this glacial dam was identified by Komatsu et al. (2009) and Batbaatar
615 and Gillespie (2016a), but they did not distinguish it as the main dam for the Darhad paleolake
616 since its elevation was considered to be much lower than the 1713 m paleolake (fig. 4). The
617 conditions for the glacial dam formation are determined by the parameters of ice-catchment and
618 the thickness of glaciers in both valleys. We think that the combining of the two glaciers in the
619 area of dam No. 4 (figs. 4, 12) in the Shishkhid Gol valley led to the stable glacier standing, thereby
620 providing a stable high backwater conditions for the formation of the Darhad paleolake at the 1713
621 m level.

622

623 **5.2 The maximum water level in the Darhad paleolake during the Late Pleistocene and lake**
624 **shoreline deformation after its drainage**

625

626 The maximum water level recorded on satellites and topographic data corresponds to 1713 m
627 asl (the western side of the Darhad Basin) and 1711 m asl (fig. 7) (the eastern side of the Darhad
628 Basin, Gillespie et al., 2008) with an uncertain level of ~1825 m pointed out by Gillespie et al.
629 (2008). The 1825 m asl level is debatable since it is not identifiable in the areal photo-
630 interpretation. All other maximum high levels in the inner water area of the paleolake are much
631 lower and vary from 1713 m asl up to 1686 m asl.
632 The difference in the elevation of the upper terrace may indicate the existence of large tectonic
633 subsidence within the Darhad Basin, which could have led to significant deformation of the
634 paleoshorelines. If the main tectonic movements took place after the drainage of the basin and the
635 terrace complex was affected, this can complicate the lake level interpretation.
636 According to (Gillespie et al., 2008), in MIS 2 there was a lake with a level of 1679 m asl. This
637 level was suggested based on the lake terrace elevation within the Jarai terminal moraine (17-19
638 ka; Gillespie et al., 2008). However, on the eastern side of the Darhad lake in the area of the Jarai
639 moraine, there are seismogenic deformations with a normal fault amplitude of 8 m (Logachev,
640 1993; Bacon et al., 2003). Thus, the 1679 m asl level may not be a true indicator of the level of the
641 paleolake, instead resulting from tectonic deformation. Moreover, beach sands with an elevation
642 of 1711 m asl (Gillespie et al., 2008), which may correspond to the 1713 level m asl on the western
643 shore of the lake, were found on a foothill slope 2 km south of the Jarai moraine. In this regard,
644 consideration of various paleolake levels can be rather complicated.
645
646 **5.3 Age and number of Darhad megafloods recorded in the Yenisei Valley**
647
648 As a result of ^{10}Be dating boulders from the surface of gravel dunes, three series of dates were
649 obtained. For analysis and their correlation with the main events of the Late Pleistocene, we present
650 a diagram with the distribution of exposure samples (^{10}Be) dating the main stages of glacier
651 advances in the East Sayan Ridge of the southern Baikal region and northern Mongolia (Gillespie

et al., 2008; Arzhannikov et al., 2012; Arzhannikov et al., 2015; Batbaatar and Gillespie, 2016b) (fig. 18 a). Another diagram shows exposure age of boulders from gravel dunes (our work), from the moraine surface in the Sarig Valley (Batbaatar and Gillespie, 2016b) and from melt water channel boulders (Gillespie et al., 2008), luminescence ages of sand units in the Darhad core, stages of the marine isotope scale (MIS), and the Darhad paleolake stages according to Gillespie et al., 2008 (fig. 18 b).

As can be seen in (fig. 18 b), series of the samples I and III correspond to MIS 3 and MIS 2. The most numerous series of the samples II is located in the transition zone between these stages. The correspondence of series I and III to the timings of the Darhad paleolake existence (17-19 ka and 35-53 ka, Gillespie et al., 2008) indicates the spatial and temporal relationship between glaciation and outburst flood events. A good example sample for the megaflood in MIS 2 is a giant boulder (8 x 4 x 2.5 m) with an age of 20.3±1.7 ka located on the 25 m terrace surface (fig. 16 j).

In our opinion, the two groups of exposure ages (samples I and III series) correspond to two megafloods that occurred in the periods 38-36 ka and 23-18 ka (fig. 18 b). This is indirectly confirmed by drilling data in the Darhad Basin. The analysis and dating of the core showed that in the periods of 34.7±8.1 and 19.5±2.6 ka, there were dramatic changes of the lake depth (the depth decreased significantly) and sands with a large proportion of the heavy fraction began to accumulate (Batbaatar and Gillespie, 2016b).

The exposure age of the samples from series II could be the result of a more complex exposure history of the boulders exhumed during the first and second megaflood events. On can propose that these boulders were not well anchored in the sediment and might have subjected to further movements or partial burial. Then when stabilized in the landscape they were exposed to cosmic rays and were able to accumulate cosmogenic nuclide until present day.

The depth of the megaflood flow in the Tuva Basin was at least 60-65 m. This is determined by the difference in the elevation of the upper terrace (fig. 14 a, b), located on the right side of the Yenisei valley and resulting from lateral erosion, and the minimum elevation of the gravel dunes

(fig. 14 c, d). The unconformity observed in alluvial deposits (fig. 16 b) on the high 30 m terraces may indicate several stages (at least two) outbursts flood from the Darhad paleolake.

We believe that the last megaflood took place in the winter or in a colder month. This is evidenced by sand blocks laid within this environment. The melting of these blocks during the warm season led to subsidence of the overlying deposits and the formation of bending deformations.

Summing up the above, we present a new vision of the Darhad paleolake formation and the Darhad megafloods. The formation and development of the Darhad paleolake coincided with the periods of glacier advance in northern Mongolia (Gillespie et al., 2008; Batbaatar et al., 2018). Based on the parameters of the two levels of the Tengis glacier (figs. 10, 11) and the distribution of lake terraces below the Tengis dam (figs. 6, 7), we can state that the Tengis glacier was not responsible for the highest stand (1713 m asl) the Darhad paleolake. The main damming role was played by a large glacier located downstream of the Tengis dam at least for the presumed highest paleolake level of 1713 m asl. The destruction of this dam occurred during periods of global warming (Batbaatar et al., 2018) which probably led to the occurrence of megafloods at least twice in MIS 3 and MIS 2. The influence of megafloods was reflected in the formation of a new erosional-depositional features (canyons, hanging valleys, gravel dunes, sand massifs, etc.) in the Yenisei valley and adjacent territories.

6. Conclusion

The studies carried out in the Darhad and Tuva basins and the dating of gravel dunes in the Yenisei valley made it possible to reconstruct the conditions of the Darhad paleolake formation and determine the stages of the Darhad outburst floods:

- satellite image interpretation and radar-derived topographic data analysis suggest significant deformations of the Darhad paleolake paleoshorelines. The maximum elevation

of the shoreline at 1711-1713 m asl, located along the periphery of the Darhad Basin, decreases to 1686 m asl in the interior of the depression. The deformation of the shoreline is associated with tectonic deformations as expressed as recent normal fault earthquakes. The deformation of the shoreline occurred after the drainage of the lake;

- lake shorelines were found on the slopes of the Shishkhid Gol valley (downstream of the Tengis Gol outlet), identical to the shorelines of the Darhad lake with a maximum elevation of 1713 m asl;
- reconstruction based on the analysis of glacial and lacustrine landforms at the Tengis Gol outlet showed that there were 2 glacier levels in MIS 2. The upper level corresponds to LGM and the lower level is later than LGM. The Tengis glacial dam, although it formed backwater, was not the main one responsible for the maximum level of the Darhad paleolake at 1713 m asl;
- analysis of remote sensing data made it possible to identify a glacial dam at the mouths of the Khara-Baryangiin and Ikh-James Gol rivers and position it as the main backwater in the formation of the highest Darhad paleolake;
- the main source of the Darhad megaflood formation was the Darhad glacial lake. The reason for the drainage of the lake was the destruction of glacial dams in the Shishkhid-Gol valley.
- in the Tuva Basin (the Yenisei valley), a series of erosion terraces was found, formed by the outburst of the Darhad paleolake. These terraces are the highwater marks indicating the maximum depth of the Darhad megaflood. The height of the upper terrace is estimated to be 100 m above the present-day water surface in the Yenisei River and 60-65 m above the surface of the lowest level of gravel dunes;
- exposure dating of boulders (^{10}Be) sampled from gravel dune surfaces in the Yenisei valley allows identifying two stages in the formation of the Darhad megaflood at 36-38 ka and 18-23 ka.

Author contributions

AS, AA, RB devised the research concept, planning, and ideas. AS, AA, participated in field work. AS took the lead in writing the manuscript. RB did the dating (10Be). GK guided the structure and editing of the results and discussion. All authors contributed to the analysis and helped shape the study.

Data availability

Geological samples are kept at the Institute of the Earth's crust SB RAS, Russia.

Declaration of competing interest

The authors declare that they have no known competing financial interests or personal relationships that could have appeared to influence the work reported in this paper.

Acknowledgments:

The reported study was funded by the Russian Foundation for Basic Research grant № 20-55-15002. Remote sensing analysis was possible thanks to the TanDEM-X project DEM_GEOL1188. The ASTER AMS national facility (CEREGE, Aix-en-Provence) is supported by the INSU/CNRS, the ANR through the “Projets thématiques d’excellence” program for the “Equipements d’excellence” ASTER-CEREGE action and IRD.

References

Arnold, M., Merchel, S., Bourlès, D.L., Braucher, R., Benedetti, L., Finkel, R.C., Aumaître, G., Gottdang, A., Klein, M., 2010. The French accelerator mass spectrometry facility ASTER: improved performance and developments. Nuclear Instruments and Methods in Physical Research B 268, 1954e1959. doi:10.1016/j.nimb.2010.02.107.

Arzhannikov, S.G., Arzhannikova, A.V., 2011. The Late Quaternary geodynamics of the Hyargas Nuur Basin and bordering scarps (western Mongolia). Russian Geology and Geophysics 52, 2, 220-229.

Arzhannikov, S.G., Braucher, R., Jolivet, M., Arzhannikova, A.V., Vassallo, R., Chauvet, A., Bourlès, D., Chauvet, F., 2012 History of late Pleistocene glaciations in the central Sayan-Tuva Upland (southern Siberia). Quaternary Science Reviews 49, 16-32.

Arzhannikov, S.G., Braucher, R., Jolivet, M., Arzhannikova, A.V., 2015. Late Pleistocene glaciations in southern East Sayan and detection of MIS 2 terminal moraines based on beryllium (^{10}Be) dating of glacier complexes. Russian Geology and Geophysics, 56, 11, 1509-1521.

Arzhannikova, A.V., Arzhannikov, S.G., Akulova, V.V., Danilova, Yu.V., Danilov, B.S., 2014. The origin of sand deposits in the South Minusa basin. Russian Geology and Geophysics 10, 1495-1508.

Batbaatar, J., and Gillespie, A.R., 2016. Outburst floods of the Maly Yenisei. Part I. International Geology Review 14, 1723-1752.

Batbaatar, J., Gillespie, A.R., 2016. Outburst floods of the Maly Yenisei. Part II – new age constraints from Darhad basin. International Geology Review 14, 1753-1779.

Batbaatar, J., Gillespie, A.R., Fink, D., Matmon, A., and Fujioka, T., 2018. Asynchronous glaciations in arid continental climate. Quaternary Science Reviews, 182, 1-19.

Bacon, S.N., Bayasgalan, A., Gillespie, A.R., Burke, R.M., 2003. Paleoseismic displacement measurements from landforms subjected to periglacial processes: observations along

781 the Jarai Gol fault near the Tamyn Am Hills, Darhad Depression, northern Mongolia. XVI Inqua
782 Congress, Abstract with Programs, 103.
783 Baker, V.R., 1973. Paleohydrology and sedimentology of Lake Missoula flooding in
784 Eastern Washington. Geological Society of America Special Paper 144, 1–79.
785 Baker, V.R., Bunker, R.C., 1985. Cataclysmic late Pleistocene flooding from Glacial Lake
786 Missoula: a review. Quaternary Science Review 4, 1–41.
787 Baker, V.R., Benito, G., and Rudoy, A.N., 1993. Paleohydrology of Late Pleistocene
788 superflooding, Altay Mountains, Siberia. Science 259, 348–350.
789 Baryshnikov, G.Ya., 1979. On the issue of the formation of large boulder alluvium of the
790 Biya River. Geology and minerals of the Altay Territory (abstracts). Barnaul, 112. (in Russian)
791 Benito, G., Thorndycraft, V., 2020. Catastrophic glacial lake outburst flooding of the
792 Patagonian Ice Sheet. Earth-Science Reviews 200, 102996.
793 Borisov, B.A., Minina, E.A., 1979. Ribbed and mesh-cellular basic moraines of the Eastern
794 Pamirs and Gorny Altay. Geomorphology 2, 69-74. (in Russian)
795 Borchers, B., Marrero, S., Balco, G., Caffee, M., Goehring, B., Lifton, N., Nishiizumi, K.,
796 Phillips, F., Schaefer, J., and Stone, J., 2016. Geological calibration of spallation production rates
797 in the CRONUS-Earth project. Quaternary Geochronology 31, 188-198.
798 Braucher, R., Guillou, V., Bourlès, D.L., Arnold, M., Aumaître, G., Keddadouche, K.,
799 Nottoli, E., 2015. Preparation of ASTER in-house 10Be/9Be standard solutions. Nuclear
800 Instruments and Methods in Physics Research, Section B: Beam Interactions with Materials and
801 Atoms 361, 335–340. doi:10.1016/j.nimb.2015.06.012
802 Braucher, R., Merchel, S., Borgomano, J., Bourlès, D.L., 2011. Production of cosmogenic
803 radionuclides at great depth: A multi element approach. Earth and Planetary Science Letters 309.
804 doi:10.1016/j.epsl.2011.06.036

Butvilovsky, V.V., 1982. On traces of catastrophic discharges of glacier-dammed lakes in the Eastern Altai. Evolution of the river systems of the Altai Territory and practical issues: Abstracts of the report for the conference, Barnaul, 12-16. (in Russian)

Butvilovsky, V.V., 1985. Catastrophic outbursts and runoff of near-glacial lakes of the South-Eastern Altai and their traces in the relief. Geomorphology 1, 65-74. (in Russian)

Carling, P.A., Kirkbride, A.D., Parnachov, S., Borodavko, P.S., Berger, G.W., 2002. Late Quaternary catastrophic flooding in the Altai Mountains of south-central Siberia: a synoptic overview and introduction to flood deposit sedimentology. In: Martini, I.P., Baker, V.R., Garzon, G. (Eds.), Flood and Megaflood Processes and Deposits: Recent and Ancient Examples. International Association of Sedimentologists Special Publication, vol. 32. Blackwell Science, London, pp. 17–35.

Chmeleff, J., von Blanckenburg, F., Kossert, K., Jakob, J., 2010. Determination of the 10Be half-life by multicollector ICP-MS and liquid scintillation counting. Nucl. Instrum. Methods Phys. Res., Sect. B 268, 192—199.

Grosswald, M.G., 1987. The last glaciation of the Sayano-Tuva highlands: morphology, feeding intensity, dammed lakes. Interaction of glaciation with the atmosphere and ocean. (Editors V.M. Kotlyakov, M.G. Grosswald) M.: Nauka, 250. (in Russian)

Grosswald, M.G., Rudoy, A.N., 1996. Quaternary ice-dammed lakes in the mountains of Siberia. Proceedings of the Academy of Sciences. Geographical series 6, 112-126. (in Russian)

Gillespie, A.R., Burke, R.M., Komatsu, G., and Bayasgalan, A., 2008. Late Pleistocene glaciers in Darhad Basin, northern Mongolia. Quaternary Research 69, 169–187.

Gosse, John C., Phillips, Fred M., 2001. Terrestrial in situ cosmogenic nuclides: theory and application. Quaternary Science Review 20, 1475—1560.

Jolivet, M., Ritz, J.-F., Vassallo, R., Larroque, C., Braucher, R., Todbileg, M., Chauvet, A., Sue, C., Arnaud, N., De Vicente, R., Arzhanikova, A., Arzhanikov, S., 2007. Mongolian summits: An uplifted, flat, old but still preserved erosion surface. Geology 10, 871–874.

831 Logachev, N.A. (Ed.), 1993. Seismotectonics and seismicity of the Khubsugul region.
832 Nauka, Novosibirsk, 184. (in Russian)
833 Komatsu, G., and Olsen, J.W., 2002. Geological and archaeological exploration of caves
834 in Mongolia. Cave and Karst Science 29, 75—86.
835 Komatsu, G., Arzhannikov, S.G., Gillespie, A.R., Burke, R. M., Miyamoto, H., Baker,
836 V.R., 2009. Quaternary paleolake formation and cataclysmic flooding along the upper Yenisei
837 River. Geomorphology 104, 143–164.
838 Komatsu, G., Baker, V.R., Arzhannikov, S.G., Gallagher, R., Arzhannikova, A.V.,
839 Murana, A., Oguchi T., 2016. Catastrophic flooding, palaeolakes, and late Quaternary drainage
840 reorganization in northern Eurasia. International Geology Review, 58, 1693-1722.
841 Korschinek, G., Bergmaier, A., Faestermann, T., Gerstmann, U.C., Knie, K., Rugel, G.,
842 Wallner, A., Dillmann, I., Dollinger, G., Lierse von Gostomski, Kossert, K., Maitia, M.,
843 Poutivtsev, M., Remmert A., 2010. A new value for the half-life of 10Be by heavy-ion elastic
844 recoil detection and liquid scintillation counting. Nucl. Instrum. Methods Phys. Res., Sect. B 268,
845 187—191.
846 Krivonogov, S.K., Sheinkman, V.S., Mistryukov, A.A., 2005. Stages in the development
847 of the Darhad dammed lake (Northern Mongolia) during the Late Pleistocene and Holocene.
848 Quaternary International 136, 83-94.
849 Margold, M., Jansen, J., Codilean, A., Preusser, F., Gurinov A., Fujioka, T., Fink D., 2018.
850 Repeated megafloods from Lake Vitim, Siberia, to the Arctic Jcean over the past 60000 years.
851 Quaternary Science Reviews 187, 41-61.
852 O'Connor, J.E., and Costa, J.E., 2004. The world's largest floods —Their causes and
853 magnitudes: U.S. Geological Survey Circular 1254: Reston, VA, U.S. Geological Survey, 13 p.
854 Perepelov, A.B., Kuzmin, M.I., Tsypukova, S.S., Demonterova, E.I., Ivanov, A.V.,
855 Shcherbakov, Yu.D., Puzankov, M.Yu., Odgerel, D., Bat-Ulzii, D., 2017. Eclogite trace in
856 evolution of late Cenozoic alkaline basalt volcanism on the southwestern flank of the Baikal Rift

857 Zone: geochemical features and geodynamic consequences. Doklady Akademii Nauk 5, 553–558.
858 (in Russian)
859 Rudoy, A.N., 1984. The giant current ripples are proof of the catastrophic outbursts of the
860 glacial lakes of the Altay Mountains. Modern geomorphological processes in the territory of the
861 Altay: Abstracts of reports. Biysk 60-64. (in Russian)
862 Rudoy, A.N., and Baker, V.R., 1993. Sedimentary effects of cataclysmic late Pleistocene
863 glacial outburst flooding, Altay Mountains, Siberia. Sedimentary Geology 85, 53–62.
864 Rudoy, A.N., 2002. Glacier-dammed lakes and geological work of glacial superfloods in
865 the Late Pleistocene, Southern Siberia, Altai Mountains. Quaternary International, 87, 119-140.
866 Selivanov, E.I., 1967. Neogen-chetverticnye ozera-giganty v Zabaikalyei Severnoi
867 Mongolii (Neogen-quaternary giant lakes in Transbaikalia and North Mongolia). Doklady AN
868 USSR 177, 175–178 (in Russian).
869 Selivanov, E.I., 1968. Spushennye ozera (Drained lakes). Priroda 3,81–82 (in Russian)
870 Spirkin, A.I., 1970. O drevnih ozerah Darhadskoi kotloviny (Zapadnoye Prihubsugulye)
871 (About ancient lakes of the Darhad depression (Western Prehovsgol)). In: Devyatkin, E.V. (Ed.),
872 Geologiya mezozoya i kainozoya Zapadnoi Mongolii (Cenozoic and Mesozoic geology of
873 Western Mongolia). Nauka, Moscow, 143–150 (in Russian)
874 Stolz, C., Hülle, D., Hilgers, A., Grunert, J., Lehmkuhl, F., and Dasc D., 2012.
875 Reconstructing fluvial, lacustrine and aeolian process dynamics in Western Mongolia. Zeitschrift
876 für Geomorphologie 3, 267–300.
877 Stone, J.O., 2000. Air pressure and cosmogenic isotope production. Journal of Geophysical
878 Research 105, 23753-23759.
879 Ufland, A.K., Iljin, A.V., Spirkin, A.I., 1969. Vpadiny baikalskogo tipa Severnoi Mongolii
880 (The Baikal-type depressions of the North Mongolia). Bulletin of the Moscow Society of
881 naturalists, Geological Series 44, 5–22. (in Russian)

882 Ufland, A.K., Iljin, A.V., Spirkin, A.I., Shilova, G.N., 1971. Osnovnye cherty stratigrafii i
883 usloviya formirovaniya kainozoiskih obrazovanii Prikosogolya (MNR) (Main features of
884 stratigaphy and formation of Cenozoic deposits in Prekosogol (MPR)). Bulletin of the Moscow
885 Society of naturalists, Geological Series 46, 54–69. (in Russian)
886 Wagner, G.A., 1998. Age determination of young rock and artifacts. Springer, 466.
887
888 **Figure captions**
889
890 Fig. 1. Locations of the three largest paleolake basins (Chuya-Kuray, Darhad, Vitim) hypothesized
891 to be the sources of megaflooding in southern Siberia. Their megaflood routs are also shown
892 (dotted lines). The bottom figure shows the study area of this article.
893 Fig. 2. The Pliocene-Quaternary history of the Darhad Paleolake development (Spirkin, 1970).
894 Fig. 3. This satellite image (Google Earth) clearly shows ancient shorelines of the Darhad
895 paleolake, located on ridge slopes.
896 Fig. 4. Interpretation of the glacial dam locations in the Shishkhid Gol valley by various authors
897 (Gillespie et al., 2008; Komatsu et al., 2009; Batbaatar and Gillespie, 2016a). Pictures and profiles
898 were built using SRTM V4 data.
899 Fig. 5. Terrace levels, gravel dunes and bars indicated on a digital elevation model (TanDEM-X
900 DEM). The red dots show sampling site locations for ^{10}Be dating (a, b, c, d). The color symbols
901 and the position of the red squares are the same as in fig. 13. Photos (e, f) show examples of dated
902 boulders.
903 Fig. 6. Satellite images a, b, c, d (Google Earth) show the locations of ancient shorelines that
904 indicate paleolake levels. All satellite images show the right bank side of the Shishkhid-Gol valley,
905 located downstream of the Tengis Gol outlet.

906 Fig. 7. The map of the Late Quaternary glaciation and locations of key study localities within the
907 Darhad paleolake and the Shishkhid Gol valley discussed in this paper. SRTM V4 data were used
908 as the base map.
909 Fig. 8. Satellite images (Google Earth) show shorelines (the location of each image is indicated in
910 Fig. 7) and their elevations are given. The variability of the lake terrace elevations along the
911 periphery of the Darhad Basin probably indicates intense tectonic deformations.
912 Fig. 9. The digital elevation model (SRTM v4) and satellite images a, b (Google Earth) show linear
913 tectonic deformation features observed in the northern part of the Darhad Basin.
914 Fig. 10. Paleogeographic reconstruction of the glacial dam in the Tengis Gol mouth, which existed
915 during the Last Glacial Maximum (MIS2). A – meltwater channel located on the right bank of
916 Tengis Gol. B - meltwater channel, located on the left bank of Tengis Gol. C - reconstruction of
917 the Tengis glacier level (left side of the mouth part of Tengis Gol) during the LGM. D - the left
918 bank of Shishkhid Gol (Sarig Gol mouth) and elements of the glacial landforms (an abraded slope
919 by the glacier and a fragment of the Tengis terminal moraine). On the digital topography map, the
920 camera symbols indicate orientations of satellite images (A, B, C, D) and the positions of the
921 topographic profiles (below) are also shown. The topographic profiles show parameters of the
922 reconstructed Tengis glacier and reflect its role in the dam formation of the Darhad paleolake. The
923 figure uses SRTM v4 data and Google Earth satellite images.
924 Fig. 11. The glacial dam reconstruction at the Tengis Gol outlet after the LGM (20-18 ka). The
925 topographic profiles show the glacier levels and the surface of the Darhad paleolake.
926 Fig. 12. Reconstruction of the glaciers that formed the Darhad paleolake dam. The Khara-
927 Baryangiin and Ikh-James glaciers network (a, b, c) is shown with the ALOS DEM. This satellite
928 image illustrates the dam area and the elevation of the meltwater channel (d).
929 Fig. 13. The photographs show a gravel dune field and a 30-meter terrace scarp capped by gravel
930 dunes (a, b). The geomorphological map is based on the interpretation of TanDEM-X DEM data,
931 revealing the nature of the erosional-depositional activity of the Darhad megaflood and Yenisei

River in Tuva Basin (c, d). The red squares are the sampling sites for ^{10}Be dating (c, d). They are shown in more detail in Fig. 5. The yellow rectangle is the location of the terraces formed by the Darhad megaflood (Fig. 14).

Fig. 14. The photographs show a complex of terraces up to 100 m high above the current Yenisei River, formed as a result the Darhad megaflood erosion (a, b). The location of high terraces in the Yenisei valley (c) and their relationship with gravel dune fields (e).

Fig.15. The photographs and satellite image (Google Earth) reveal the morphology and structure of gravel dunes distributed in the Yenisei valley (a, b, c).

Fig. 16. Sedimentary complex of various fractions, formed in the Yenisei Valley as results of the erosion-depositional activity of the Darhad megaflood (a, b, d, e, f, j, h, g) and aeolian processes (c).

Fig. 17. Plot of the in-situ exposure age (^{10}Be) distribution obtained from the boulders within gravel dunes of the Yenisei River valley.

Fig. 18. Plot (a) displays the exposure ages of glacial deposits of the Eastern Sayan Ridge and northern Mongolia. Plot (b) shows three peaks of exposure ages (^{10}Be) associated with two Darhad megafloods and one with the loss of ^{10}Be atoms due to changes in boulder exposure during the second Darhad megaflood event. The red circles indicate the ages of significant change in the fraction of the Darhad paleolake deposits. The green circles show the exposure ages of the maximum advance of the Tengis glacier (LGM MIS2). The white circles show the formation ages of the meltwater channels.

Table 1. Description of samples dated by ^{10}Be cosmogenic nuclides.

Figure

Click here to access/download;Figure;fig 1.jpg

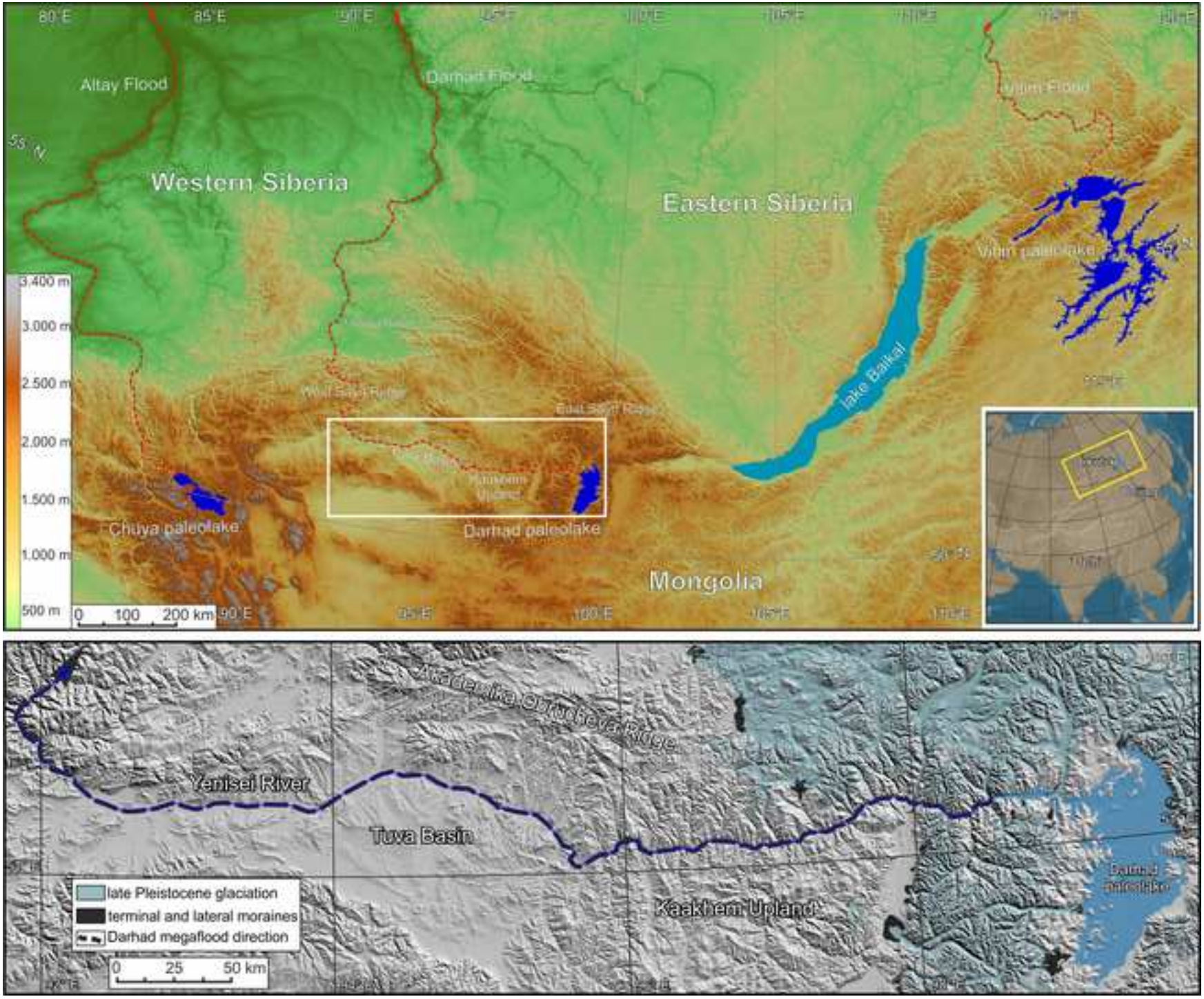

Figure

Click here to access/download;Figure;fig 2.jpg

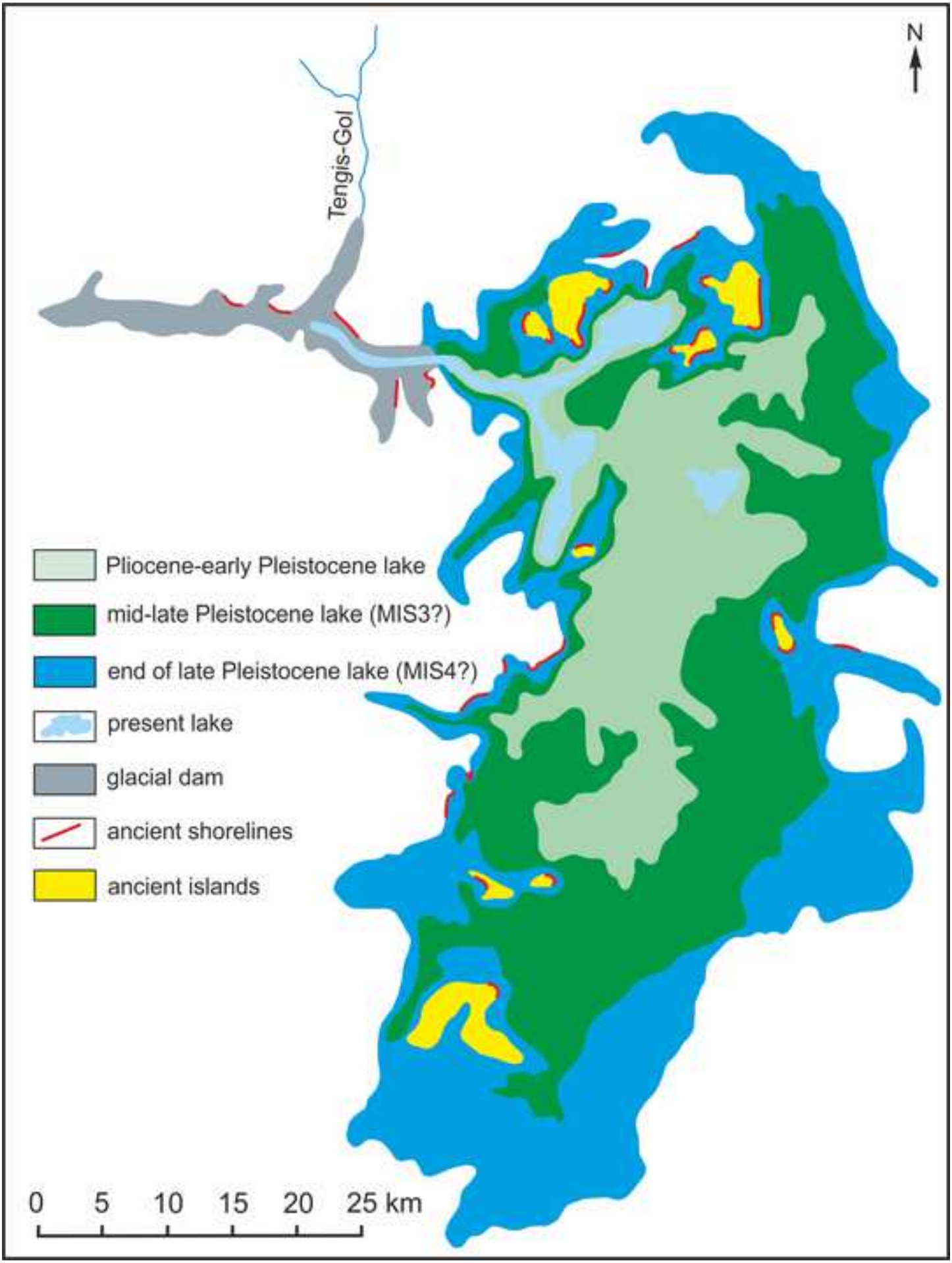

Figure

Click here to access/download;Figure;fig 3.jpg

Figure

Click here to access/download;Figure;fig 4.jpg

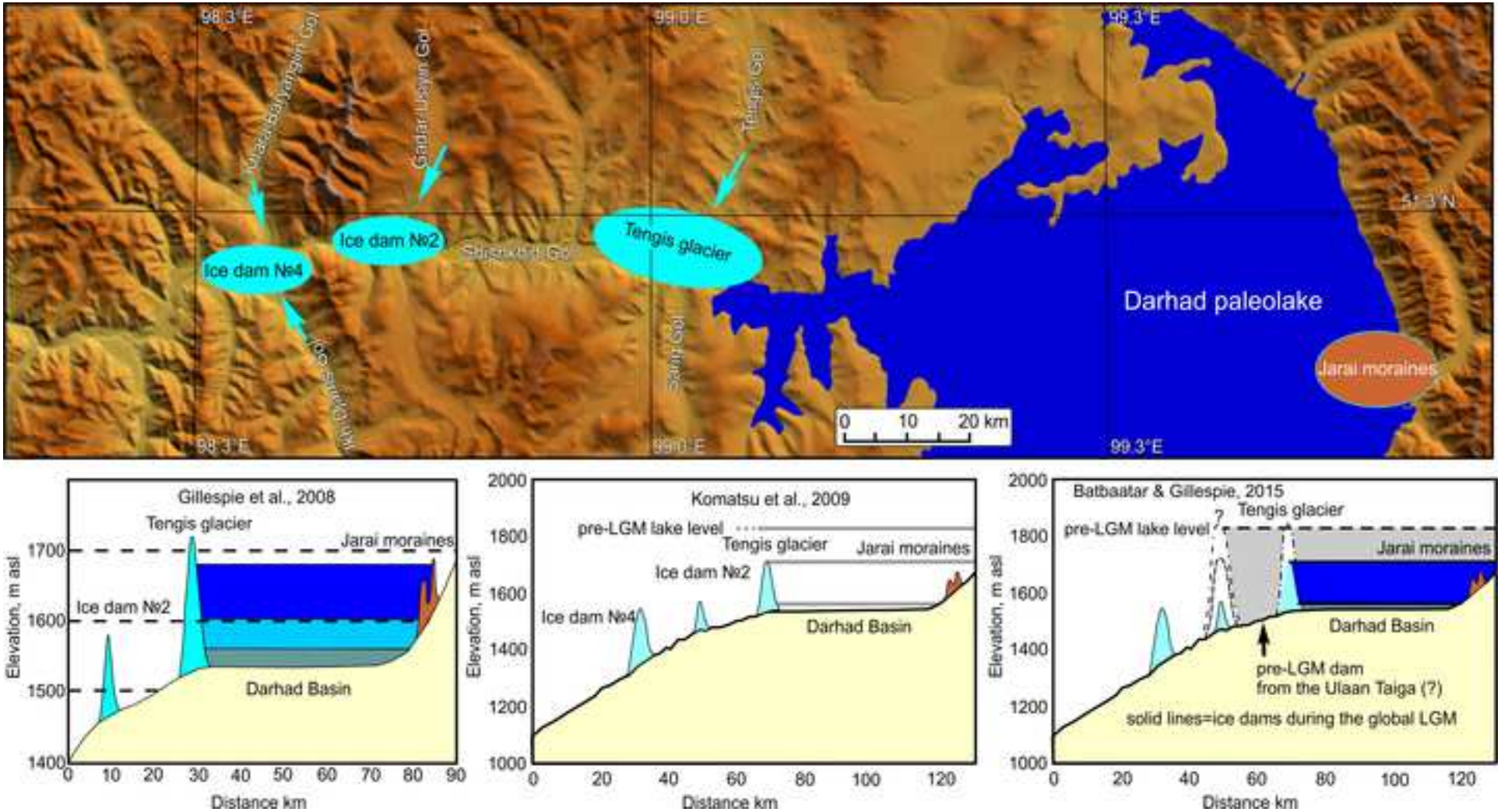

Figure

Click here to access/download;Figure;fig 5.jpg

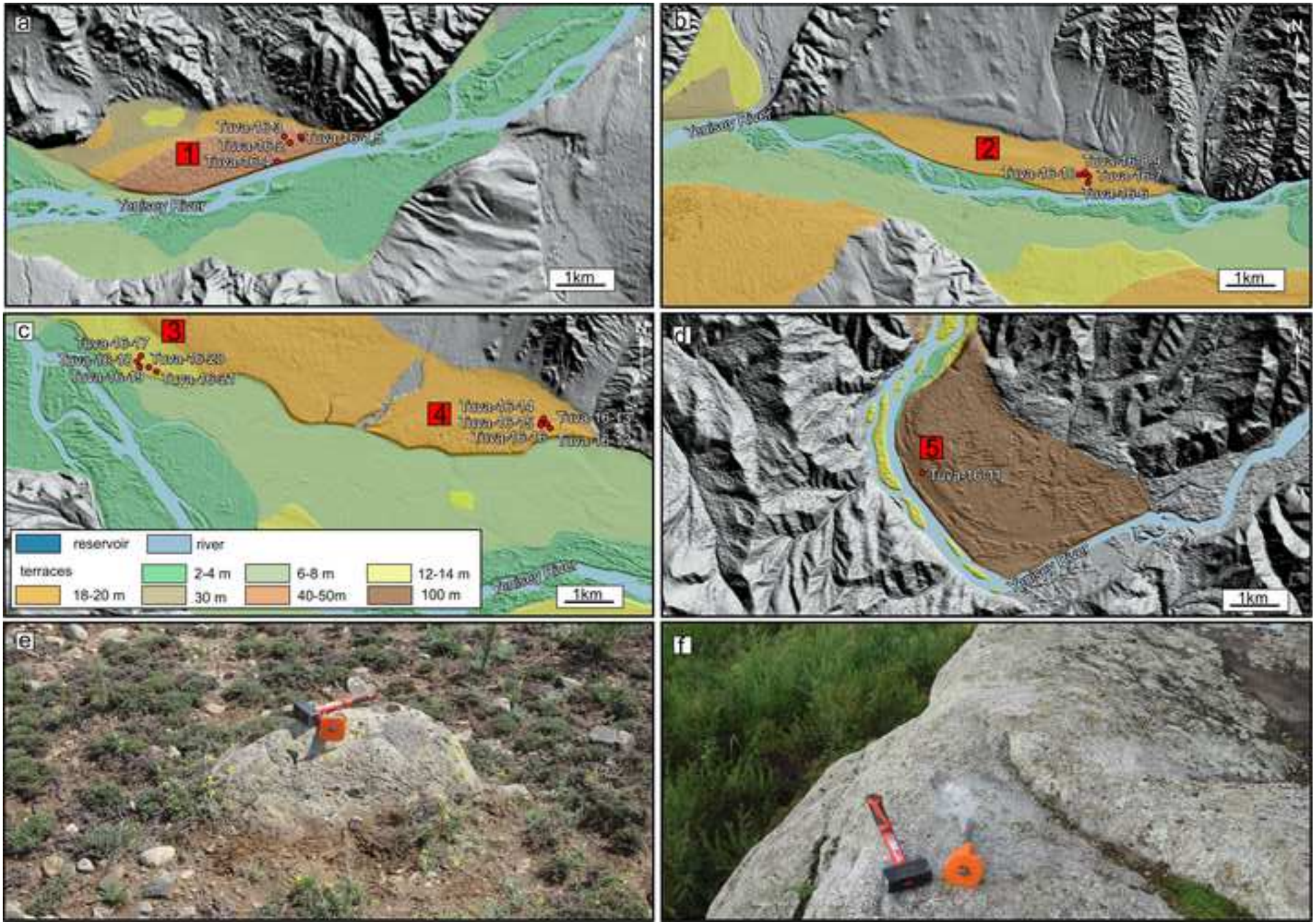

Figure

Click here to access/download;Figure;fig 6.jpg

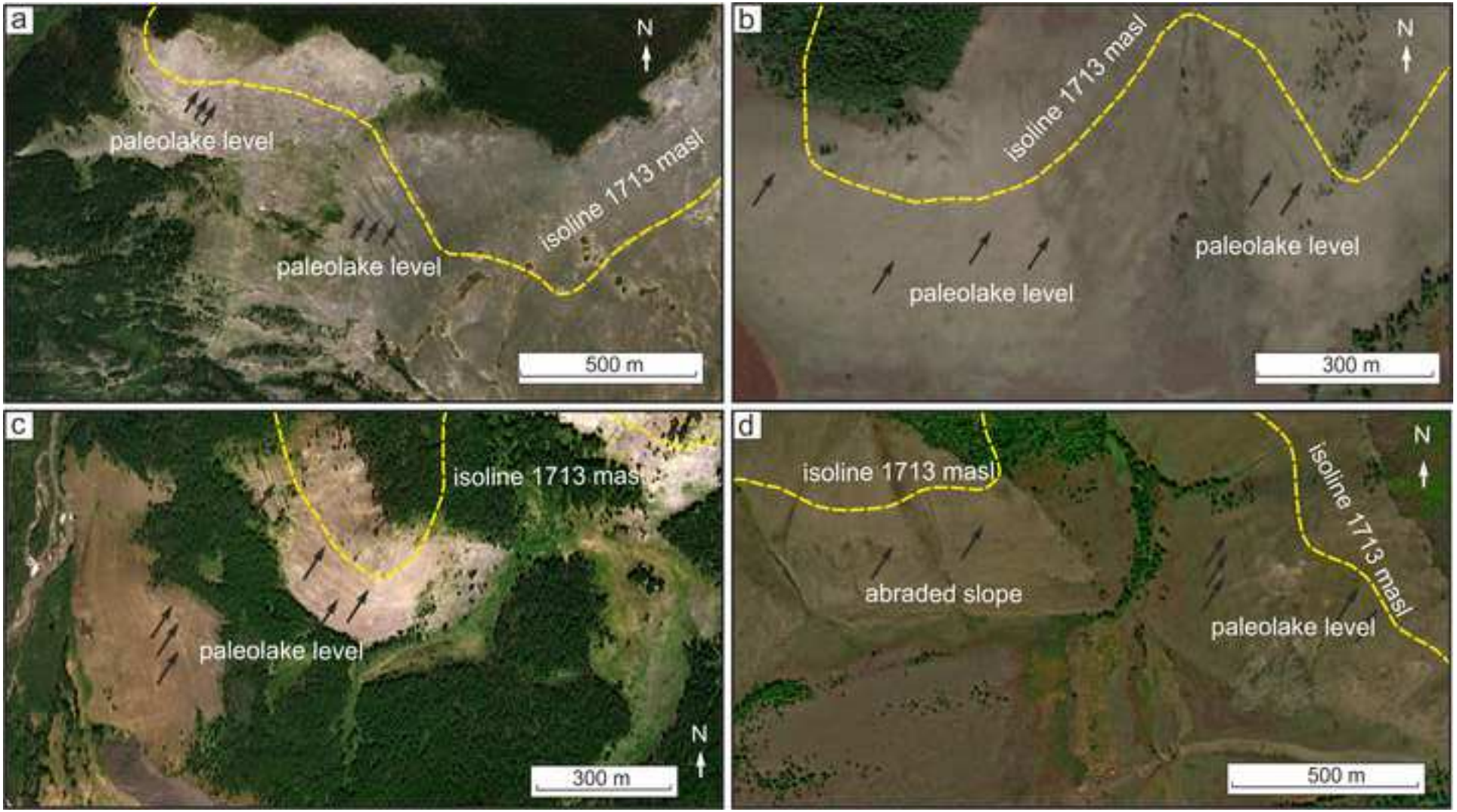

Figure

Click here to access/download;Figure;fig 7.jpg

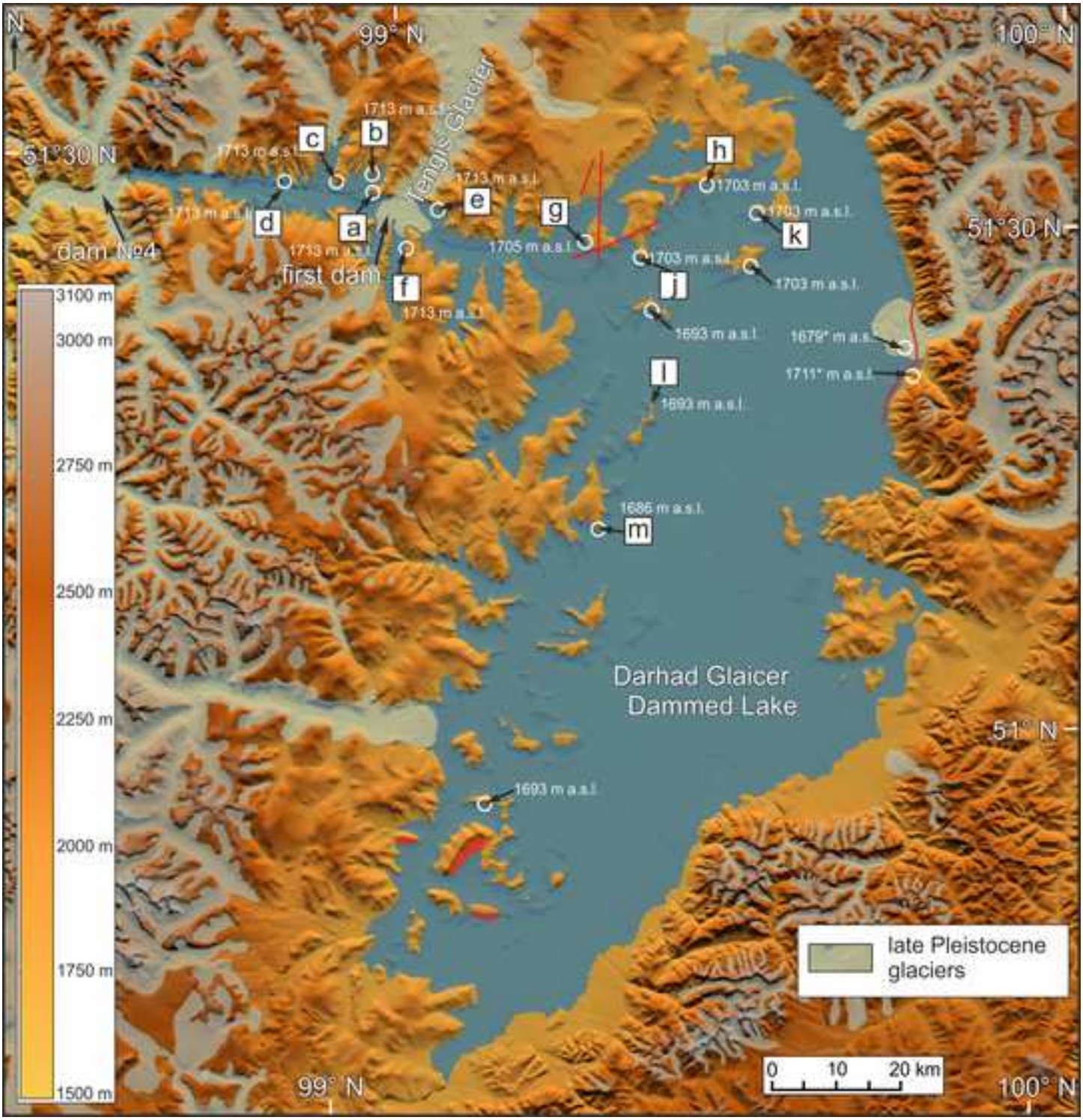

Figure

Click here to access/download;Figure;fig 8.jpg

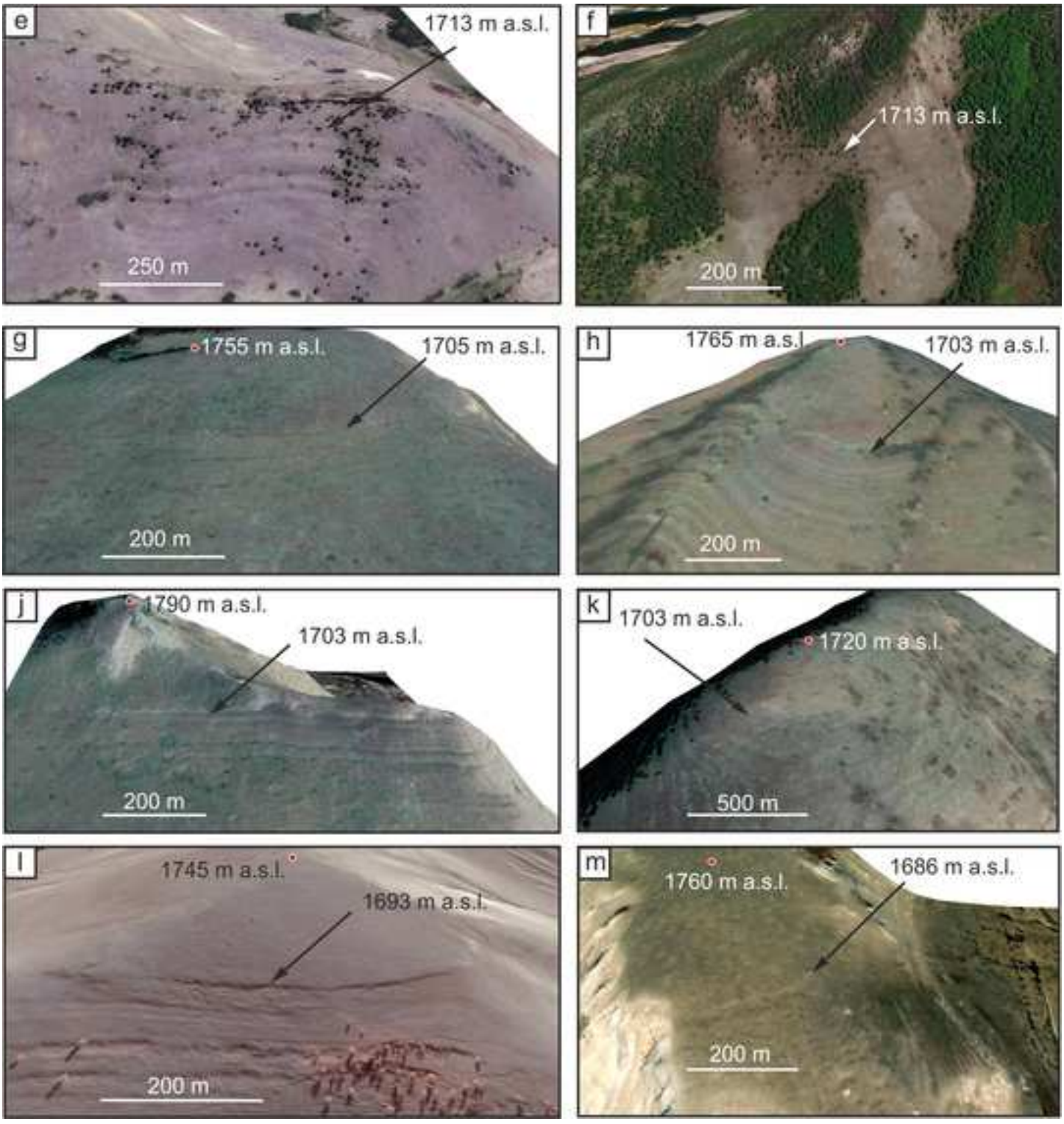

Figure

Click here to access/download;Figure;fig 9.jpg

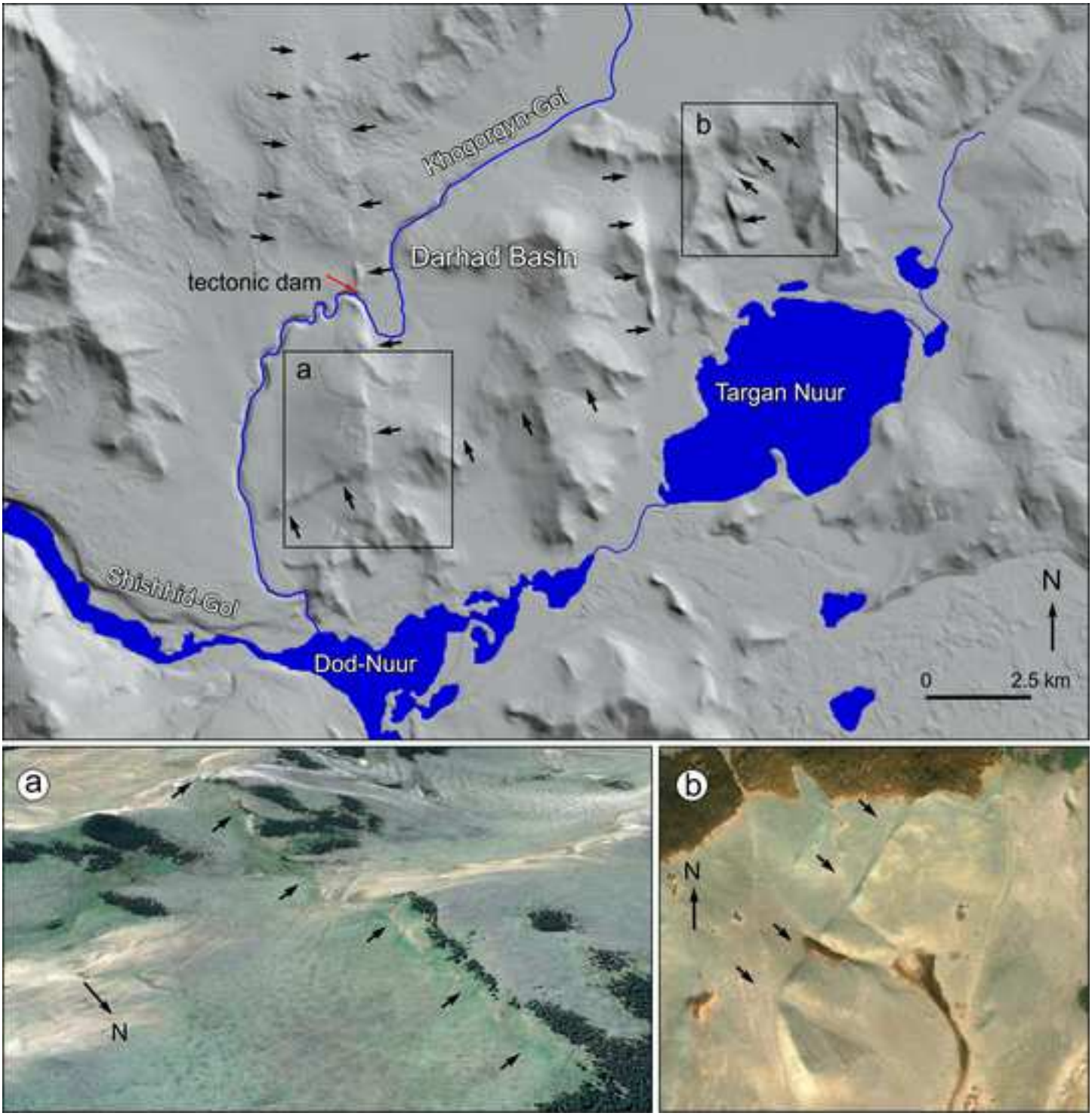

Figure

Click here to access/download;Figure;fig 10.jpg

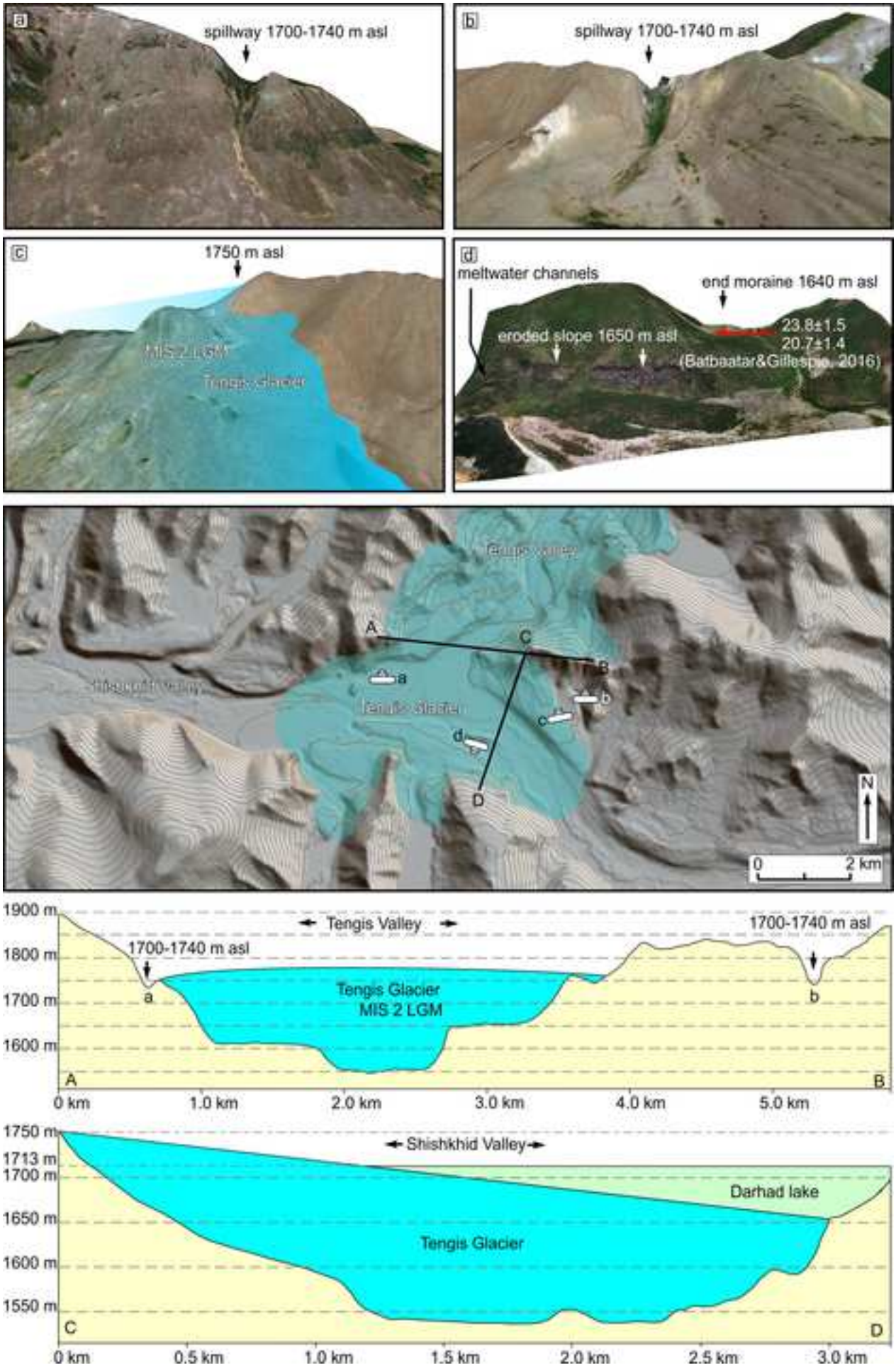

Figure

Click here to access/download;Figure;fig 11.jpg

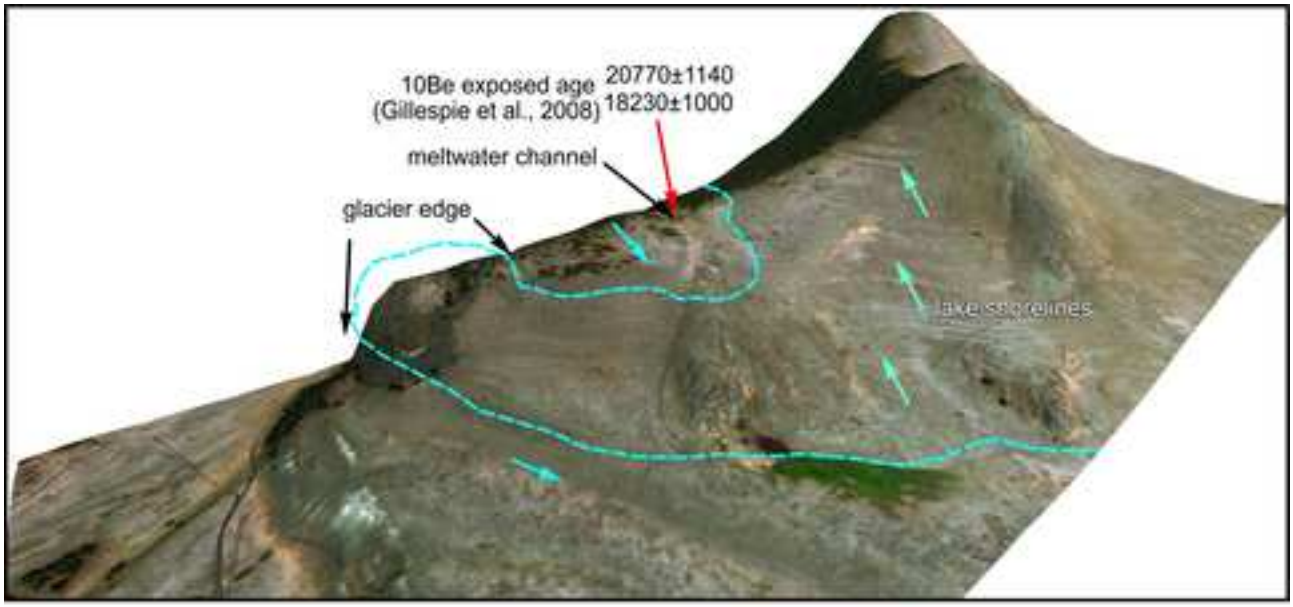

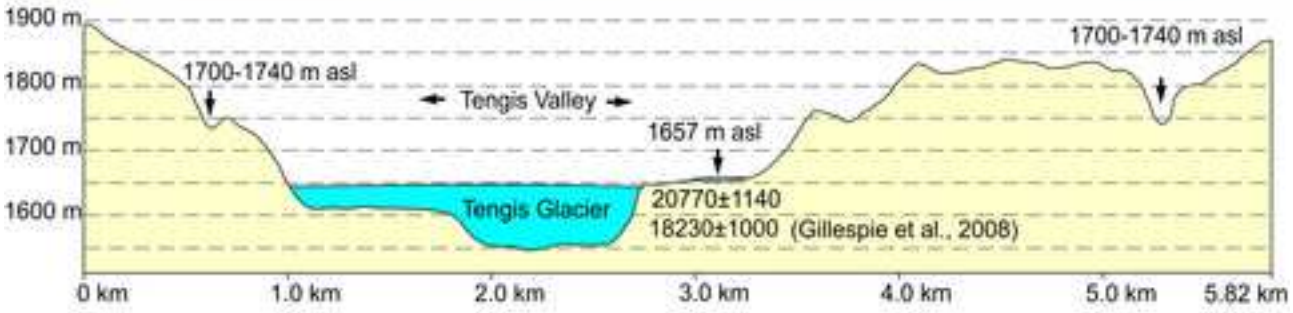

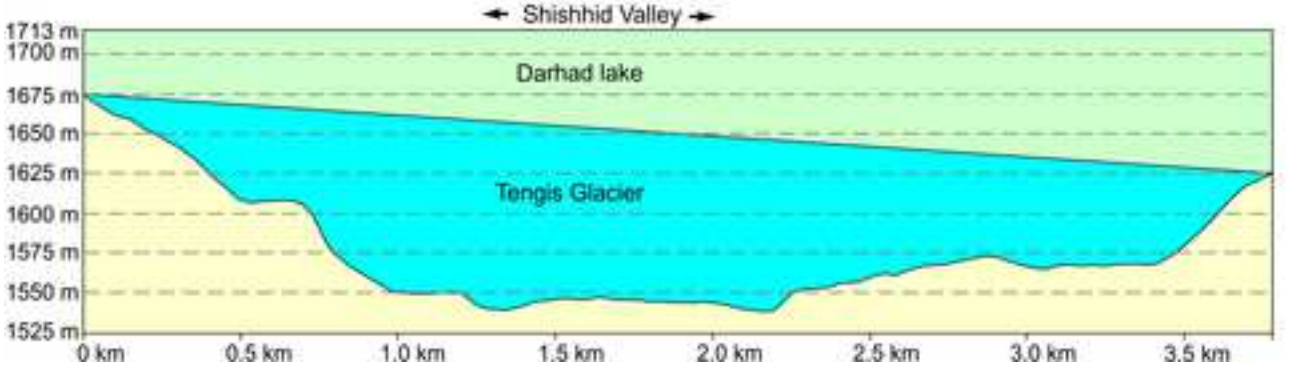

Figure

Click here to access/download;Figure;fig 12.jpg

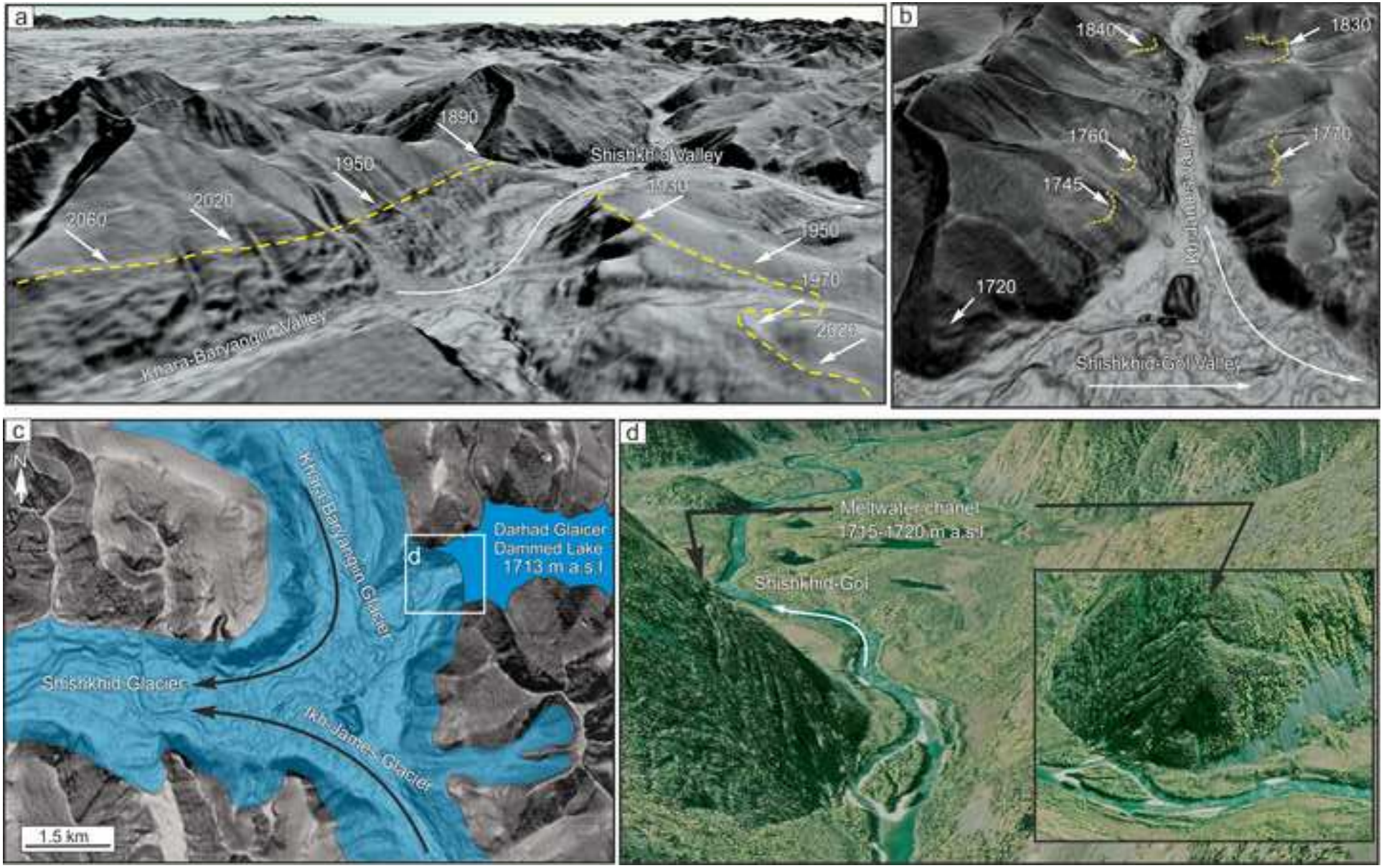

Figure

Click here to access/download;Figure;fig 13.jpg

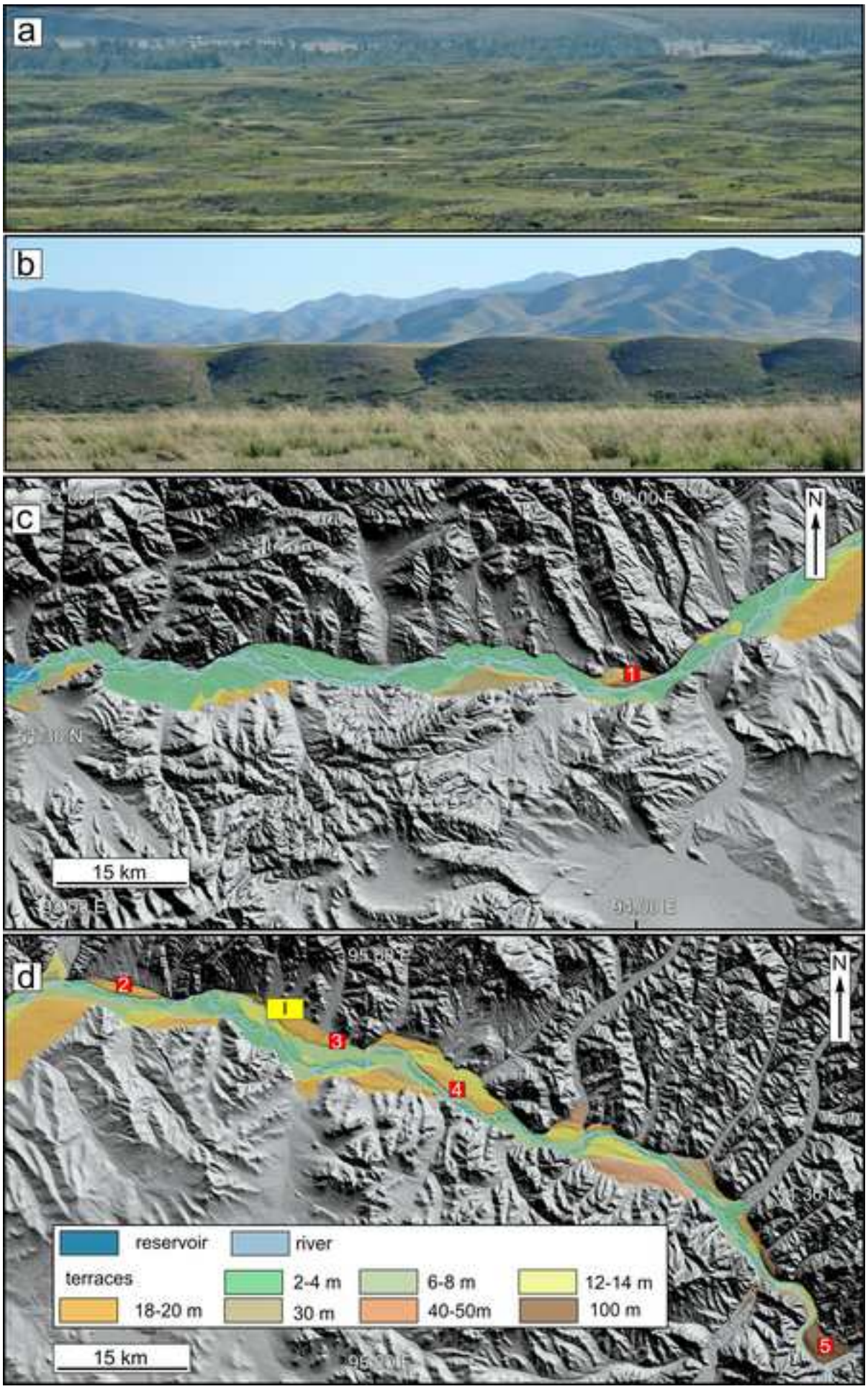

Figure

Click here to access/download;Figure;fig 14.jpg

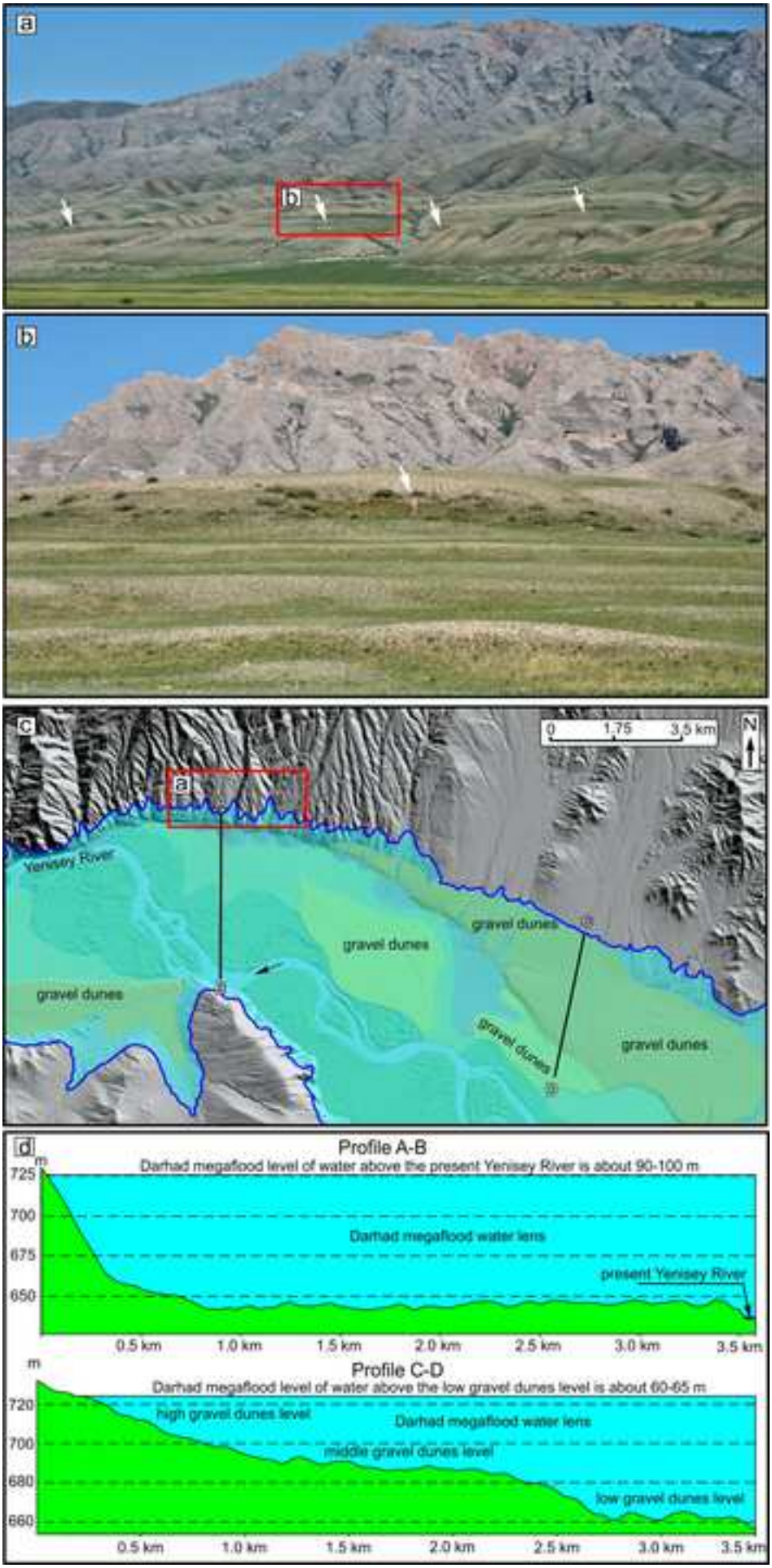

Figure

Click here to access/download;Figure;fig 15.jpg

Figure

Click here to access/download;Figure;fig 16.jpg

Figure

Click here to access/download;Figure;fig 17.jpg

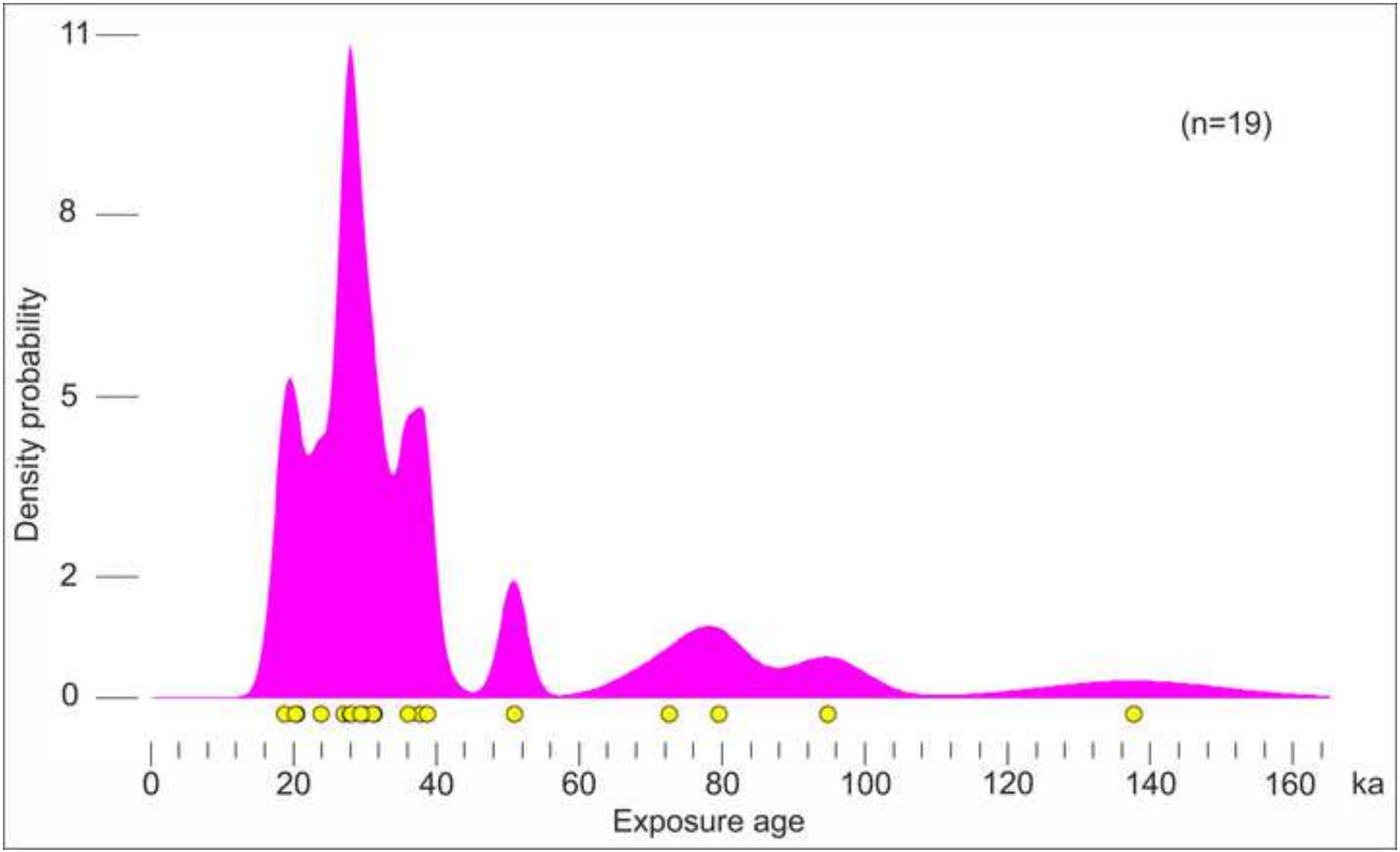

Figure

Click here to access/download;Figure;fig 18.jpg

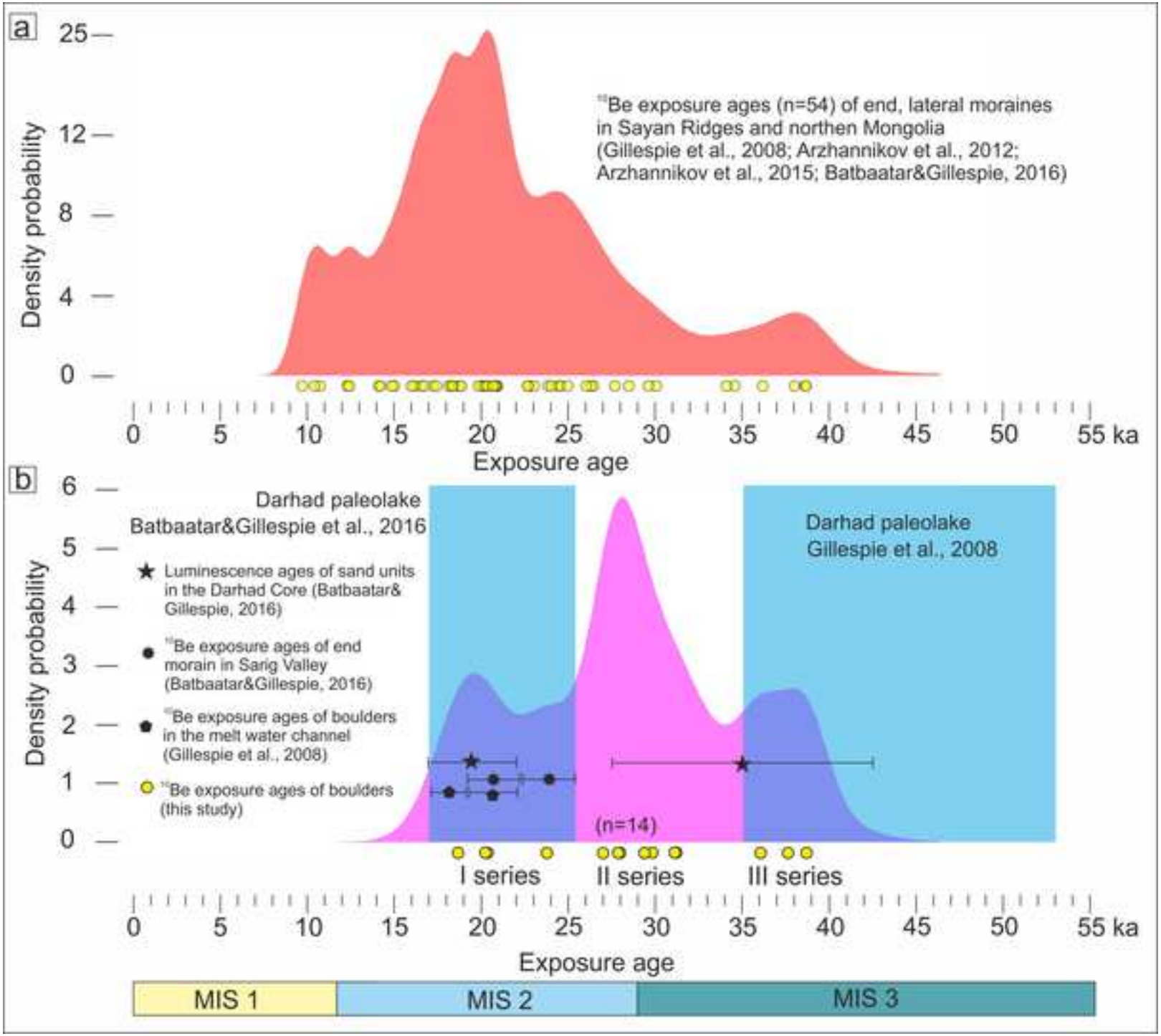

Sample	Latitude (N) (decimal degrees)	Longitude (E) (decimal degrees)	Altitude (m asl)	10Be (at/g)	Uncert	Min Age (yr)	Uncert (yr)
T1	51.567367	94.015250	624	574 981	32 819	79 536	4 540
T3	51.568117	94.008667	629	230 402	15 215	31 360	2 071
T4	51.562050	94.006050	623	218 543	20 945	29 811	2 857
T5	51.567367	94.015250	624	980 548	92 456	137 574	12 972
T6	51.710217	94.597467	661	234 350	20 058	31 142	2 665
T7	51.711283	94.596950	669	205 506	11 750	26 983	1 543
T8	51.711900	94.595433	663	284 043	23 740	37 607	3 143
T9	51.711900	94.595433	663	141 539	12 459	18 645	1 641
T10	51.712017	94.594450	662	210 779	12 929	27 840	1 708
T11	51.306617	95.739583	748	165 882	14 300	20 352	1 755
T12	51.652917	94.945500	687	216 061	9 741	27 944	1 260
T13	51.653350	51.653350	690	157 924	20 011	20 211	2 561
T14	51.653483	94.943017	688	721 106	41 889	94 723	5 503
T15	51.653483	94.943017	688	391 622	14 766	50 893	1 919
T16	51.653483	94.943017	688	278 197	10 534	36 021	1 364
T17	51.665917	94.839617	662	543 193	47 323	72 613	6 326
T18	51.665017	94.838800	660	179 750	10 322	23 767	1 365
T19	51.664567	94.839050	660	291 188	9 448	38 646	1 254
T20	51,6642667	94.841383	655	220 694	17 442	29 348	2 319

Samples have a density of 2.5 and are ~3 cm thick. Samples were crushed, sieved (0.5-1mm) and chemically etched. Pure quartz was dissolved in HF in the presence of ^{9}Be carrier (100 µg of 3.025 x 10-3 g/g ^{9}Be solution). Ion exchange columns (Dowex 1x8 and 50Wx8) were used to extract ^{10}Be. ^{10}Be/^{9}Be ratios were measured by accelerator mass spectrometry at ASTER the French National Facility (CEREGE, Aix en Provence). Concentrations are reported relative to NIST SRM4325 standard, using an assigned value for the ^{10}Be/^{9}Be ratio of 2.79×10^{-11} and a ^{10}Be half-life of 1.387 Ma (Korschinek et al., 2010). A sea level high latitude spallation production rate of 4.49 ± 0.29 atoms g^{-1} y^{-1} and the stone scaling factors (Stone, 2000) were applied. Muons scheme is based on Braucheret et al., (2003).

Declaration of interests

☒The authors declare that they have no known competing financial interests or personal relationships that could have appeared to influence the work reported in this paper.

☐The authors declare the following financial interests/personal relationships which may be considered as potential competing interests:

Author Agreement Statement

We the undersigned declare that this manuscript is original, has not been published before and is not currently being considered for publication elsewhere. We confirm that the manuscript has been read and approved by all named authors and that there are no other persons who satisfied the criteria for authorship but are not listed. We further confirm that the order of authors listed in the manuscript has been approved by all of us. We understand that the Corresponding Author is the sole contact for the Editorial process. Arzhannikov S. is responsible for communicating with the other authors about progress, submissions of revisions and final approval of proofs Signed by all authors as follows:

Arzhannikov S.

Arzhannikova A.

Regis Braucher

Goro Komatsu

Credit Author Statement

AS, AA, RB devised the research concept, planning, and ideas. AS, AA, participated in field work. AS took the lead in writing the manuscript. RB did the dating (10Be). GK guided the structure and editing of the results and discussion. All authors contributed to the analysis and helped shape the study.